Hyaluronan Nanoplatelets Exert an Intrinsic Antiinflammatory Activity in a Rat Model of Bladder Painful Syndrome/Interstitial Cystitis

Raul Diaz-Salmeron, Catherine Cailleau, Stéphanie Denis, Gilles Ponchel, Kawthar Bouchemal

Hyaluronan Nanoplatelets Exert an Intrinsic Anti-inflammatory Activity in a Rat Model of Bladder Painful Syndrome/Interstitial Cystitis

*Raul Diaz-Salmeron [1], Catherine Cailleau [1], Stéphanie Denis [1], Gilles Ponchel [1], Kawthar Bouchemal [2]**

1. Université Paris-Saclay, CNRS UMR 8612, IGPS, 91400 Orsay, France

2. Chimie ParisTech, PSL University, CNRS, Institut de Recherche de Chimie Paris, 75005 Paris, France

*Corresponding author

kawthar.bouchemal@chimieparistech.psl.eu

Abstract

Glycosaminoglycan (GAG) replenishment therapy consists of the instillation of GAG solutions directly in the bladder to alleviate Bladder Painful Syndrome/Interstitial Cystitis (BPS/IC). However, several issues were reported with this strategy because the GAG solutions are rapidly eliminated from the bladder by spontaneous voiding, and GAG have low bioadhesive behaviors. Herein, GAG nanomaterials with typical flattened morphology were obtained by a self-assembly process. The formation mechanism of those nanomaterials, denoted as nanoplatelets, involves the interaction of α-cyclodextrin cavity and alkyl chains covalently grafted on the GAG. Three GAG were used in this investigation, hyaluronan (HA), chondroitin sulfate (CS), and heparin (HEP). HA NP showed the best anti-inflammatory activity in an LPS-induced in vitro inflammation model of macrophages. They also exhibited the best therapeutic efficacy in a BPS/IC rat inflammation model. Histological examinations of the bladders revealed that HA NP significantly reduced bladder inflammation and regenerated the bladder mucosa. This investigation could open new perspectives to alleviate BPS/IC through GAG replenishment therapy.

Keywords: Hyaluronic acid; Nanoparticles; Nanoplatelets; Self-assemblies; Bladder.

Abbreviations

α-CD: α-cyclodextrin

BPS/IC: Bladder Painful Syndrome/Interstitial Cystitis

CS: Chondroitin sulfate

CS-ODA: *N*-octadecylamine-chondroitin sulfate

Cy5.5: Cyanine 5.5-NH_2

DMF: Dimethylformamide

DMSO: Dimethyl sulfoxide

EDC: 1-ethyl-3-(3-dimethylaminopropyl) carbodiimide

GAG: Glycosaminoglycan

ATR-FTIR: Fourier transform infrared spectroscopy

HA: Hyaluronan

HA-PA: *O*-palmitoyl hyaluronan

HEP: Heparin

HEP-ODA: *N*-octadecylamine-heparin

HUCs: Human Urothelial Cells

IC_{50}: the concentration of GAG preparations to reduce cell viability by 50% relative to untreated control cells

IC_{30}: the concentration of GAG preparations to reduce cell viability by 70% relative to untreated control cells

J774A.1: Murine monocyte macrophages

LPS: lipopolysaccharide

NHS: *N*-hydroxysuccinimide

NMR: Nuclear Magnetic Resonance

NPs: Nanoplatelets

ODA: Octadecylamine

PA: palmitic acid

PMN: polymorphonuclear neutrophils

SEM: Scanning Electron Microscopy

TEM: Transmission Electron Microscopy

1. Introduction

Bladder Painful Syndrome/ Interstitial Cystitis (BPS/IC) is a heterogeneous, multifactorial, and chronic disease syndrome characterized by permanent urinary symptoms such as pelvic and perineal pain, urinary frequency, and urgency.[1] The etiology is unknown, but several theories have been proposed.[2] The most widely accepted is the increase in the permeability of the bladder urothelium due to the loss of the protective glycosaminoglycan (GAG) layer located at the urothelium surface. Because the GAG layer is the primary origin of the permeability barrier of the bladder,[3, 4] after removing the GAG layer, urothelial permeability increases.[5] The urothelium becomes permeable to urinary irritants, toxic substances, and pathogens.[4, 6] Current treatment strategies, such as cystectomy or intravesical instillation of drug solutions or suspensions directly into the bladder, have been evaluated at a clinical level. However, the challenging diagnosis of the disease makes it difficult to find an effective treatment. Nowadays, the most effective therapy for treating BPS/IC consists of GAG replenishment therapies.[7] Indeed, an HA solution administered in the bladder is the first-line treatment of BPS/IC.[8] Chondroitin sulfate (CS) and heparin (HEP), a sulfated polysaccharide that has a structural similarity to GAG, were also used to alleviate BPS/IC.[9]

However, drug efficacy is limited by several factors, including low permeability of the urothelium to hydrophilic macromolecules such as HA, CS, and HEP, and drug dilution and washout during the bladder filling and voiding.[10] Consequently, repeated intravesical instillations are required to reach local therapeutic concentrations. Those instillations may be performed under general anesthesia by a clinical practitioner and could often cause pain in patients. Therefore, there is a real clinical need to investigate new formulations involving and leading to increased local drug concentrations close to the urothelium and a decrease in the frequency of intravesical instillations. In this context, a class of flattened and hexagonal-shaped nanoparticles composed of polysaccharides has been developed by Bouchemal and coworkers.[11-16] These nanoparticles, called nanoplatelets (NP), are prepared by the hierarchical supramolecular self-assembling of a hydrophobically modified polysaccharide, such as HA,[12-14] HEP,[17] CS,[16] dextran, amylopectin, pullulan,[18] or chitosan,[11, 19] and α-cyclodextrin (α-CD) molecules. These NP are as soft as hydrogels from their Young's modulus (380 kPa).[13] Recent results demonstrated that NP are better internalized by macrophages[13] and show faster diffusion in water[12] than native polysaccharides. In a recent study,[14] it was demonstrated that the NP are rapidly attached to the mucosa at a lower concentration than nanospheres, even though the two types of particles had comparable surface potentials. Interestingly, the *in vivo* bioaccumulation and bioelimination studies revealed that the NP are eliminated from the rat bladder mucosa less rapidly than the nanospheres.[14] The hypothesis on which this work is built is that NP flat

morphology, fast diffusion in biological fluids, and high mucoadhesion could be advantageous for treating BPS/IC. Herein, the anti-inflammatory activity of NP composed of HA, CS, and HEP was investigated *in vitro* on macrophages, on urothelial cells, and *in vivo* on a rat model of BPS/IC. The results were compared to native GAG and suspensions of hydrophobically modified GAG.

2. Materials

2.1. Reagents

HA (M_w $\sim 51 \times 10^3$ g mol^{-1} according to the manufacturer) was purchased from LifeCore Biomedical (Minnesota, USA). CS from shark cartilage (M_w $\sim 40 \times 10^3$ g mol^{-1} evaluated by Polyacrylamide Gel Electrophoresis),[16] and HEP (M_w $\sim 40 \times 10^3$ g mol^{-1} according to the manufacturer) were obtained from TCI Europe (Zwijndrecht, Belgium). Palmitoyl chloride, deuterium oxide, 1-ethyl-3-(3-dimethylaminopropyl) carbodiimide (EDC), *N*-hydroxysuccinimide (NHS), formamide, octadecylamine (ODA), *E. coli* lipopolysaccharide (LPS), protamine sulfate (PS), α-CD, phosphate-buffered saline (PBS, pH$\sim 7.0 - 7.3$), dexamethasone phosphate, diethyl ether, 4% paraformaldehyde solution, and anhydrous pyridine were purchased from Sigma Aldrich (St. Quentin Fallavier, France). Methanol, ethanol, acetone, dimethylformamide (DMF), anhydrous dichloromethane (DCM), and dimethylsulfoxide (DMSO) were obtained from Carlo Erba Reagents (Val de Reuil, France). Cyanine 5.5-NH_2 (Cy5.5, λ_{ex} 679 nm, λ_{em} 705 nm) was purchased from Lumiprobe (Montluçon, France). PD10 desalting columns (Sephadex G-25) were from GE Healthcare Life Sciences (Amersham, UK). ELISA MAX^{TM} standard Set detection kit was from Biolegend (San Diego, USA). For animal experiments, Zoletil® 100 was purchased from Virbac (Carros, France), xylazine 2% was obtained from Interchemie werken (Venray, Netherlands). Dialysis membranes were purchased from Spectra/Por (Biovalley, Marne la Vallée, France). Milli-Q® water was used for all the experiments (Resistivity 18.2 MΩ.cm at 21 °C, Millipore purification system, Millex, SLAP 0225, Millipore, France).

2.2. Reagents for cell culture

Primary human urothelial cells (HUCs) were obtained from ScienCell, and murine hematopoiesis-derived macrophages (J774A.1) were from CLS (Eppelheim, Germany). Culture media Roswell Park Memorial Institute 1640 (RPMI 1640) and urothelial growth medium were from ThermoFisher Scientific (Illkirch, France). Fetal bovine serum, sterile penicillin/streptomycin solution, 3-[4,5- dimethylthiazol-2-yl]-2,5-diphenyl tetrazolium bromide (MTT), and calcein-AM were from Sigma Aldrich (St. Quentin Fallavier, France). Penicillin/streptomycin solution contains

10,000 units of penicillin and streptomycin dissolved in a citrate buffer at a concentration of 10 mg mL^{-1}.

2.3. Animals

Adult female Wistar rats (9-12-week-old females $\sim 250 - 300$ g, Janvier Labs, St. Berthevin, France) were housed in a standard controlled environment at 22 °C, 60% relative humidity, a 12-h light/12-h dark cycle with lights on at 8 am, and access to food and water *ad libitum*. This study was conducted following the ethical standards approved by the Animal Ethics Committee of the University of Paris Saclay following EU Directive 2010/63/EU for animal experiments (agreement N°15378-2018060610295653).

3. Methods

3.1. Hydrophobization of CS and HEP by amide bonds

The hydrophobization of CS and HEP using an amide link was performed by grafting ODA on the carboxylic acid groups on the polysaccharides. Protocols previously optimized for CS were adapted.[16] Two degrees of substitutions (DS) were investigated.

For the low degree of substitution ($DS_{1:1}$), 7.5 mL of formamide was added to a 25 mL three-neck balloon containing 500 mg of CS (0.93 mmol of disaccharide units) or HEP (0.43 mmol of disaccharide units). The GAG were dissolved in formamide at 60 °C under vigorous magnetic stirring (1000 rpm, for 1 h, under reflux). Once fully dissolved, the mixture was cooled at 25 °C. Then, EDC (178 mg for CS and 82 mg for HEP) was dissolved in 2 mL of DMF and added to the mixture containing CS or HEP. The weights of EDC were calculated to obtain a molar ratio of 1:1 between polysaccharide carboxylic groups and EDC. Then, ODA (251 mg for CS and 116 mg for HEP) were dispersed in 4 mL of DMF and added to the EDC/GAG mixtures. After 24 h of magnetic stirring (750 rpm) at 25 °C, the hydrophobically modified GAG were precipitated in acetone (160 mL), followed by a magnetic stirring for 90 min to dissolve unreacted ODA.[16] The precipitate was filtrated under a vacuum (filter porosity n°2) and washed three times with acetone. Then, the hydrophobically modified GAG were dried under a vacuum for 24 h. The powders were dispersed in 40 mL of water and dialyzed (molecular weight cutoff 10^3 g mol^{-1}) against 1 L of water for 72 h. Water used for dialysis was replaced five times every day. The dialyzed compound was then freeze-dried for 24 h (Alpha 1-2 freeze-dryer, Fisher Scientific Bioblock, Illkirch, France). The obtained hydrophobically modified CS and HEP are denoted *N*-octadecylamine-chondroitin sulfate (CS-ODA) and *N*-octadecylamine-heparin (HEP-ODA).

For the high degree of substitution ($DS_{1:3}$) of hydrophobically modified CS and HEP, the same protocol was used by increasing the weights of EDC and ODA. The weights of EDC and ODA were calculated to provide a 1:3 molar ratio between the disaccharide unit and EDC or ODA, respectively. Briefly, EDC (535 mg for CS and 248 mg for HEP) was dissolved in 2 mL of DMF. The weighted amount of EDC was calculated to reach a molar ratio 1:3 between polysaccharide carboxylic groups and EDC. ODA (752 mg for CS and 348 mg for HEP) was dispersed in 4 mL of DMF and added to the mixture.

3.2. Hydrophobization of CS, HEP, and HA by ester bonds

The hydrophobization of the sulfated GAG (CS and HEP) by an ester link was performed by reacting palmitoyl chloride on polysaccharide hydroxyl groups according to the protocols previously optimized for HEP.[17] Briefly, 1 g of CS (1.9 mmol of disaccharide units) or HEP (0.86 mmol of disaccharide units) were suspended in 11 mL of anhydrous DCM contained in a 250 mL tri neck flask and heated at 60 °C under magnetic stirring (400 rpm). Anhydrous pyridine (5 mL) was added, followed by an excess of palmitoyl chloride (5.3 g for CS and 2.5 g for HEP) dissolved in 6 mL anhydrous DMF under continuous magnetic stirring at 60 °C for two hours and one hour at 20 °C. The weight of palmitoyl chloride was calculated according to a protocol previously optimized for the ester link of HEP[17] to provide a 1:10 molar ratio between the disaccharide unit and palmitoyl chloride.

Then, 100 mL of cold ethanol (at 4 °C) was added. The precipitates were collected and centrifuged for 10 min at 4000 rpm at 25 °C. Then, the supernatants were removed, and the precipitates containing the hydrophobic compounds were collected and washed once with ethanol and twice with diethyl ether. The precipitates were then collected, centrifuged for 10 min at 4000 rpm at 25 °C, and dried under a vacuum for 24 h. The powders were then dispersed in 40 mL of water and dialyzed against 1 L of water for 72 h (molecular weight cutoff 10^3 g mol^{-1}). Water was replaced five times every day. The dialyzed compound was then freeze-dried for 24 h. The obtained hydrophobically modified CS and HEP are denoted *O*-palmitoyl-chondroitin sulfate (CS-PA) and *O*-palmitoyl-heparin (HEP-PA).

O-palmitoyl-hyaluronan (HA-PA) esterification protocol was adapted from Diaz-Salmeron et al.[15] Briefly, one molar equivalent of HA (400 mg) was suspended in 20 mL of dry DMF at 20 °C. Then two molar equivalents of palmitoyl chloride (549.68 mg) in 2 mL of dry DMF were added to the HA suspension and reacted under magnetic stirring for three days at room temperature. The molar ratio was selected according to previous work.[15] After 72 h of reaction, the *O*-palmitoyl HA was precipitated by adding 20 mL of methanol. After that, the mixture was purified by two cycles of

washing/centrifugation with acetone for 15 min at 4000 rpm. The lower part was dried under a vacuum for 24 h and then dialyzed for three days against 2 L of water with a dialysis membrane (molecular weight cutoff 10^3 g mol^{-1}). Water was replaced five times per day. The dialyzed compound was freeze-dried for 24 h.

3.3. Chemical coupling of a Cy5.5 on hydrophobically modified and native GAG

Chemical coupling of Cy5.5 on hydrophobically modified GAG or native GAG was performed by adapting previously published protocols.[15] Briefly, 25 mg of hydrophobically modified GAG or native GAG were dissolved in water to reach a concentration of 19 mM. Then, an EDC/NHS solution of 40 mM respectively in water was added to the polysaccharide solution. The reaction mixture was stirred at room temperature for 30 min to activate GAG carboxylic groups. Afterward, a Cy5.5 solution in DMSO (0.45 mM) was prepared and added to the GAG mixture dropwise under magnetic stirring. The reaction was allowed to continue for 12 h at room temperature, protected from light. After 12 h of stirring, the reaction mixture was purified by dialysis followed by lyophilization. Dialysis was performed using a dialysis membrane (molecular weight cutoff 10^3 g mol^{-1}) against 1 L of water for 24 h by changing the water five times. Lyophilization for 24 h to obtain a solid-state powder. The final purification step to eliminate unreacted molecule dye involves the re-dispersion of the powder in water, followed by a purification with a PD10 desalting column. Water was used as the mobile phase. The final product was lyophilized again to obtain a stable solid and purified product.

3.4. Chemical characterizations of the hydrophobically modified compounds

Infrared spectra were obtained with a Fourier transform infrared spectroscopy spectrometer (ATR-FTIR, PerkinElmer FT-IR Spectrometer Spectrum Two) equipped with a diamond reflection accessory embedded into a ZnSe support and operating at $4\ \mathrm{cm}^{-1}$ resolution. Fifty scans were accumulated in each run and referred to air. The resultant spectra were analyzed by Perkin Elmer software (Spectrum Version 10.03)

Nuclear magnetic resonance (^{1}H-NMR) was performed using a Bruker Avance 300 Spectrometer (operating at 300 MHz) to confirm the grafting of hydrophobic chains on CS and HEP. Samples were prepared by dissolving polymers (10 mg) in a deuterated solvent (1 mL).

For elemental analysis characterizations, total carbon, hydrogen, nitrogen, oxygen, and sulfur present in modified and native CS and HEP were determined using an Analyzer LECO SC144 (Service Central d'Analyse du CNRS, Vernaison, France). Briefly, 15 mg of each compound were burned at 1350°C over oxygen flux. The degree of substitution corresponding to the number of

hydrophobic chains grafted on 100 disaccharide units of GAG was calculated following Equation (S1) for CS and HEP and Equation (S2) for HA (Supporting Information).[15]

3.5. NP preparation

The NP suspensions were prepared by adding in a small vial 10 mg of each modified polysaccharide and 100 mg of α-CD powder. The weight was then brought up to 1 g with water. Each preparation was mixed at room temperature under magnetic stirring for 72 h.

3.6. Preparation of controls

Hydrophobically modified GAG suspensions in water were prepared according to the same protocol used for NP, without adding α-CD. Solutions containing native GAG were freshly prepared by mixing GAG powders (10 mg) in water (1 mL).

3.7. NP morphological characterizations

The surface potentials of the NP and the suspensions of hydrophobically modified polysaccharides were characterized by zeta potential measurements. The zeta potentials were calculated at 25 °C by measuring the electrophoretic mobility using an electrophoretic light scattering technique (Zetasizer Nanoseries Nano-ZS, Malvern Instruments, France). The scattered angle was 173°. The suspensions were diluted to 1:33 v/v in NaCl (1 mM). Measurements were performed on three independent formulations.

Transmission electron microscopy (TEM) characterizations were performed at 80 kV transmission using a transmission electron microscope (JEOL1400) coupled to TEM Domain Center software. The suspensions were diluted in water (1/30) and manually homogenized for sample preparation. This dilution was optimized to observe the particles with good contrast. Then, 4 µL were placed on a grid and dried for 5 min. The grid was disposed on a slide and inserted in the microscope for analysis.

A high-resolution scanning electron microscope (SEM) equipped with a field emission gun electron source was performed with a Zeiss Merlin Compact microscope operating at 10 kV on samples obtained by deposing liquid dispersions directly on double face carbon scotch fixed on a brass stub. Suspensions were diluted with water (1/30) and dried at room temperature for 24 h before observations.

3.8. Cell culture and cell viability analysis

Cells (macrophages and HUC) were maintained at 37 °C in a humidified atmosphere (5% CO_2). HUC were cultured in a serum-free urothelial cell medium supplemented with penicillin/streptomycine solution. The urothelial cell growth was conducted in poly-L-lysine coated culture vessels (2 µg cm^{-2}). Macrophages were cultured in RPMI 1640 medium supplemented with 10% fetal bovine serum and 1% of penicillin/streptomycin solution.

In vitro cytotoxicity of CS, HEP, or HA preparations was investigated using the MTT assay. Cells were seeded in 100 µL of the corresponding culture medium (2×10^5 cells mL^{-1}) in 96-well plates and preincubated for 24 h at 37 °C. Then, 100 µL of each GAG preparation were diluted in culture media to reach the following GAG concentrations: 0.01, 0.1, 1, 10, 25, 50, 100, 250, and 500 µg mL^{-1}. After 24 h of incubation, 20 µL of an MTT solution in PBS (5 mg mL^{-1}) were added to each well. After 4 h or 90 min incubation for HUCs and macrophages, the culture medium was gently aspirated, and 200 µL of DMSO were added to dissolve formazan crystals. Then, 96-well plates were stirred at 450 rpm for 30 min. After that, the absorbances of solubilized formazan crystals were measured with a microplate reader at 570 nm. The percentage of cell viability in each well was calculated as the absorbance ratio between treated and untreated control cells. IC_{50} and IC_{30} values (the concentration of each preparation to reduce cell viability by 50% and 70% relative to untreated control cells, respectively) were calculated from the dose-response curve. All experiments were repeated 6 times.

3.9. Evaluation of the GAG anti-inflammatory activity

GAG anti-inflammatory activity was evaluated in vitro on macrophages. Cells were seeded in 24-well plates at a cellular density of 2×10^4 cells per well in the culture medium and were incubated for 48 h until 80% confluency at 37 °C and 5% CO_2. Then, the medium was removed and replaced by fresh medium alone (negative control of inflammation) or fresh medium with LPS at 1 µg mL^{-1} to induce inflammation. Plates were incubated for 3 h at 37 °C and 5% CO_2. Afterward, GAG preparations were added to each well at a concentration of 25 µg mL^{-1}. The selected GAG concentrations were higher than the IC_{50}. Free dexamethasone phosphate was used as a reference anti-inflammatory drug at the same GAG concentration. Macrophages treated with PBS were used as a positive control of inflammation.

After 24 h of incubation with the treatment, cell supernatants were collected and frozen at −80 °C until analysis was performed. Mouse inflammatory cytokine IL-6 was quantified using an ELISA standard set detection kit. Each sample was diluted 1/50 with fresh culture medium for a final

volume of 100 µL. Standard solutions ($7.8 - 500\ mg\ mL^{-1}$) were also diluted in the same conditions. Cytokine results were analyzed and fitted to an asymmetric sigmoidal 5PL curve with GraphPad Prism software. All measurements were performed in triplicate.

3.10. PS/LPS induced BPS/IC rat model

At day zero, rats were anesthetized intraperitoneally with a mixed solution of Zoletil® 100 at a concentration of 50 mg mL^{-1} (15 mg kg^{-1}) and xylazine 2% (1 mg kg^{-1}). After anesthesia, rats were catheterized with a soft catheter PE25 attached to a syringe coupled to a 22 Ga needle. The bladder was emptied and washed two times with sterile PBS. Animals were then instilled in the bladder through the catheter with protamine sulfate (10 mg mL^{-1} in sterile PBS, 500 µL). The syringe was removed, but the catheter was maintained and closed with a screw cap. After 45 min, the bladder was emptied again, and LPS (1 mg mL^{-1} in sterile PBS; 500 µL) was subsequently instilled through the catheter for 30 min. Afterward, the bladder was emptied and washed two times with sterile PBS. Subsequently, 500 µL of each treatment formulation was intravesical instilled for one hour. Then, the catheter was removed, and animals were allowed to recover from the anesthesia effects. Each treatment group consisted of six rats. Three rats were used for the in vivo imaging to evaluate the bioaccumulation and the bioelimination for three days after the treatment. After three days, the other three animals were used for the inflammation and histological evaluation of the bladder.

3.11. Evaluation of the residence time of the formulations in rat bladders

The residence time of the formulations in rat bladders was determined *in vivo* after intravesical instillation of fluorescently labeled formulations (500 µL, 10 mg mL^{-1} containing 0.15% of Cy5.5) or PBS (used as a negative control) in healthy rats ($n = 3$ animals per group) and rats bearing LPS-induced inflammation. The residence time of each formulation was recorded at 0, 3, 6, 24, 48, and 72 h with an IVIS Lumina LT Series III System (Caliper Life Sciences) using a 660 nm excitation laser and a 710 nm emission filter. During imaging experiments, the animals were kept under anesthesia with 3% isoflurane in oxygen flow (1 L min^{-1}) during the imaging stage. The abdomen regions of rats were shaved before imaging. The fluorescent signals' images and measurements were acquired and analyzed with Living Imaging software. A manual threshold was selected for each image to measure the averaged radiant efficiency. Fluorescent background signals using a 580 nm excitation laser and a 710 nm emission filter were subtracted from the fluorescent signal using the same selected threshold in both images.

3.12. Evaluation of the inflammation of GAG by histological analysis

At the end of the residence time study, the anesthetized rats were euthanized, and the bladders were removed and split longitudinally. Then, they were fixed for 24 h in 4% paraformaldehyde and embedded in paraffin blocks. Then, 4-µm sections were stained with haematoxylin-eosin-safran (HES). The severity of inflammation in bladder tissues was evaluated by scoring it in six high-power fields (15 × magnification) based on four criteria: venous congestion and hemorrhage, edema, cell infiltration, and urothelium damage. The score for every histopathological feature was summed to the others for each animal.

Venous congestion and hemorrhage. 0: non-dilated vessels; 1: focal, small, dilated vessels; 2: diffuse, small, dilated vessels, hemorrhage; 3: diffuse small, dilated vessels with focal large, dilated vessels and hemorrhage; 4: diffuse small, dilated vessels with diffuse large, dilated vessels and hemorrhage.

Edema. 0: absence; 1: mild focal edema, 2: moderate focal edema, 3: moderate diffuse edema, 4: moderate diffuse edema with architectural distortion

Cellular infiltration (neutrophils and monocytes). 0: no cellular infiltration; 1: mild focal lymphoid infiltration (< 10 cells), 2: diffuse mild lymphoid infiltration ($10 - 40$ cells), 3: diffuse moderate lymphoid infiltration ($40 - 100$ cells), 4: diffuse moderate lymphoid infiltration with dense lymphoid aggregates (> 100 cells).

Urothelium damage. 0: no injury, 1: minimal injury without ulceration or hemorrhaging, 2 mild injuries with mild ulceration, 3: moderate injury (loss of urothelium), 4: severe injury with loss of urothelium, ulceration, and hemorrhaging.

Bladder tissues from 3 rats per treatment group were randomly chosen for histological analysis. Each bladder tissue was observed and analyzed six times on six different high-magnification fields (15 × magnification). HES-stained tissues were scored from 0 to 4 on a blinded test.

3.13. Statistical analyses

Statistical analyses were performed using GraphPad Prism Version 7.0 software. The normality of all experimental values was examined with a Shapiro-Wilk test. Cytokine production values obtained in vivo, the fluorescence signal after administration of the formulations in the rat bladder, and global inflammation scores were statistically examined with a two-way Kruskal-Wallis test followed by a Tukey's multiple comparison post-test. The level of significance for all statistical analyses was set at a p-value < 0.05. The size distributions obtained by TEM and SEM were fitted to

normal gaussian law. TEM and SEM size measurements were reported as the amplitude, the mean size, and the standard deviation. The box-plot representation of the distribution curves —that is recommended for both large and small data series since practically all the values are shown — was applied to compare NP diameter histograms.

4. Results and discussion

4.1. Chemical hydrophobization of GAG

This study investigated three types of GAG: CS, HEP, and HA. The alkyl chains were grafted through an amide or an ester link for each GAG. FT-IR spectra for native and hydrophobically modified GAG were shown in the supplementary data (Figure S1-S5, Supporting Information). Native CS (Figure S1 and S3, Supporting Information), HEP (Figure S2 and S4, Supporting Information), and HA (Figure S5, Supporting Information) exhibited characteristic IR spectra with well-defined and assigned absorption bands.[16, 17] The broad band between $3000-3500\ \mathrm{cm^{-1}}$ corresponds to the $\mathrm{O-H}$ stretching vibrations overlapped with $\mathrm{N-H}$ stretching vibrations of *N*-acetyl side chains. The bands at $1611-1614\ \mathrm{cm^{-1}}$ were assigned to the antisymmetric stretching vibration of carboxylic acids on CS, HEP, and HA. The amide II vibration mode in position 2 of GlcNAc ($\mathrm{C-N}$ stretching coupled to $\mathrm{C-N-H}$ bending) of CS and HA was detected at $1551\ \mathrm{cm^{-1}}$ and $1559\ \mathrm{cm^{-1}}$, respectively. The band at $1409-1415\ \mathrm{cm^{-1}}$ was assigned to the symmetrical vibration of free $\mathrm{COO^-}$ groups for the three polysaccharides. The $1376\ \mathrm{cm^{-1}}$ feature was associated with the symmetrical bending vibration of $-\mathrm{CH_3}$ of *N*-acetyl groups and the $\mathrm{O-H}$ variable angle vibration. The peak at $1257\ \mathrm{cm^{-1}}$ due to the stretching vibration of $\mathrm{C-N}$ bonds of amide groups is the characteristic absorption peak of CS. The intense features at $1225\ \mathrm{cm^{-1}}$ and $1067\ \mathrm{cm^{-1}}$ were assigned to the antisymmetric and symmetric stretching vibration of $\mathrm{S=O}$ bonds in sulfate groups of CS and HEP, respectively. The shoulder at $1062\ \mathrm{cm^{-1}}$ was set to the symmetrical stretching mode of $\mathrm{S=O}$ bonds in sulfate groups of CS and HEP. The peaks at $1130\ \mathrm{cm^{-1}}$ and $1031\ \mathrm{cm^{-1}}$ were attributed to the antisymmetric stretching vibrations of $\mathrm{C-O-S}$ and $\mathrm{C-O-C}$, respectively. Finally, the absorption band at $996\ \mathrm{cm^{-1}}$ could be assigned to $\mathrm{CO-NH}$ plan vibration.

A comparison of the FTIR spectra of CS and HEP with CS-ODA and HEP-ODA, respectively, confirmed the grafting of ODA in both polysaccharides (Figure S1 and Figure S2, Supporting Information). Characteristic bands of $\mathrm{CH_2}$ and $\mathrm{CH_3}$ groups of ODA were detected. The peak at $1467\ \mathrm{cm^{-1}}$ corresponds to $\mathrm{C-H}$ bending mode vibration of the ODA methylene group, while the increase in the peak intensity at $1382-1390\ \mathrm{cm^{-1}}$ corresponds to the symmetrical bending mode of methyl groups. Intense bands appeared in the range of $2800-2900\ \mathrm{cm^{-1}}$ ($\mathrm{C-H}$ antisymmetric

and symmetric stretching of CH_2 and CH_3 groups), corresponding to the vibration of aliphatic chains. The grafting of ODA on carboxylate groups on CS and HEP results in a significant decrease in the band intensity of the carboxylate groups at $1614\ cm^{-1}$. The peak corresponding to the carboxylate groups at $1409\ cm^{-1}$ disappeared for CS-ODA and decreased for HEP-ODA. The spectra of CS-ODA and HEP-ODA were characterized by the appearance of the absorbance peaks characteristic of amides. Two bands appeared at $1692\ cm^{-1}$ and $1567\ cm^{-1}$, corresponding to amide I and II stretching vibration for CS-ODA, while only a band appeared at $1680\ cm^{-1}$, corresponding to amide II stretching vibration in HEP-ODA.

The grafting of the palmitoyl chain on CS, HEP, and HA via an ester link was also confirmed from the infrared spectra analysis (Figures S1-S5, Supporting Information). In comparison with the CS, HEP, and HA spectra, the spectra of hydrophobically modified polysaccharides by ester links showed three additional peaks (Figures S3-S5, Supporting Information). The peak signal between $2800\ cm^{-1}$ and $2900\ cm^{-1}$ strongly increased. The peak signal was attributed to the stretching vibrations of the $C-H$ bounds of $-CH_2$ and $-CH_3$ groups of the palmitoyl chains grafted on the polysaccharides. The infrared spectra of CS-PA and HEP-PA were characterized by the appearance of peaks at $1804\ cm^{-1}$ and $1741\ cm^{-1}$ for CS-PA, at $1799\ cm^{-1}$ and $1742\ cm^{-1}$ for HEP, and at $1730\ cm^{-1}$ for HA. Those peaks were attributed to carbonyl groups of ester functions.

Elemental analysis revealed an increase in the molar ratio of C/S and C/O for all the hydrophobically modified GAG (Table 1). The degrees of substitutions corresponding to the number of hydrophobic chains grafted on 100 disaccharide units of CS, HEP, or HA were calculated from elemental analysis results (DS_{EA}) and from ^{1}H-NMR spectra (DS_{NMR}) by integrating the characteristic signals of alkyl chain protons[20] in Figure S6 in the Supporting Information. Details on the peak assignments of alkyl chains were reported in our previous work.[15] The results in Table 1 revealed that the DS_{NMR} was in the same range as those obtained from elemental analysis. The DS varied from 0.12% to 5.42%. For the following sections, the results of the DS will be expressed by NMR results.

Table 1. Degrees of substitutions of different hydrophobically-modify compounds were calculated by elemental analysis (DS_{EA}) and ^{1}H-NMR (DS_{NMR}).

Sample	C mol%	H mol%	N mol%	O mol%	S mol%	C/S mol%	C/O mol%	DS_{EA}* (%)	**DS_{NMR} (%)
CS	2.38	4.89	0.24	3.10	0.13	17.92	0.77	-	-
CS-ODA DS_{High}	3.11	6.37	0.35	2.58	0.13	25.40	1.21	6.55	5.42
CS-ODA DS_{Low}	2.88	5.84	0.38	2.81	0.15	18.09	1.02	0.15	0.12
CS-PA	2.45	5.00	0.20	3.02	0.13	18.21	0.81	0.22	0.25
HEP	1.76	3.86	0.13	2.97	0.25	7.07	0.59	-	-
HEP-ODA DS_{High}	2.89	6.15	0.30	2.55	0.24	12.25	1.13	4.53	3.25
HEP-ODA DS_{Low}	2.14	4.49	0.24	2.97	0.28	7.44	0.72	0.31	0.28
HEP-PA	1.9	4.05	0.14	3.08	0.26	7.33	0.62	0.20	0.15
HA	6.07	5.68	0.44	6.09	0	-	1.00	-	-
HA-PA	6.33	5.94	0.60	5.55	0	-	1.14	0.14	0.12

*Equation S1 for sulfated GAG and Equation S2 for HA in the Supporting Information.
**DS calculated from ^{1}H NMR by integrating the characteristic signals of alkyl chain protons[20] in Figure S6 in the Supporting Information.

4.2. NP physicochemical characterizations

Once characterized, the hydrophobically modified GAG were magnetically mixed with an aqueous solution of α-CD to obtain the NP. As previously optimized, the concentrations of α-CD and hydrophobically modified GAG were maintained at 10 wt% and 1 wt%, respectively.[15-17] Once mixed, the alkyl chain of the hydrophobically modified GAG interacts with the α-CD cavity through a sequential binding.[18] The stoichiometry of the interaction between the alkyl chains and the α-CD cavity was characterized by isothermal titration microcalorimetry[18] and by quantifying unreacted α-CD.[16] Results showed that two α-CD molecules interact with palmitoyl groups,[18] while three α-CDs interact with ODA chains grafted on the polysaccharide.[16] Then, the inclusion complexes self-assemble in a columnar organization as represented in the Supporting Information (Figure S57 and Figure S58). The columnar organization was characterized by X-ray diffraction.[11, 21] Indeed, the columnar organization (also called channel organization) is characterized by a strong reflection at $2\theta = 20°$.[11, 21]

Herein, to understand whether the GAG hydrophobization through an ester link or an amide link affects the NP morphology, either palmitic acid (PA) or ODA was covalently grafted on the GAG chain. The obtained NP were characterized by measuring the zeta potentials and by TEM and SEM observations. TEM and SEM observations revealed the presence of well-structured NP that have a typical hexagonal morphology and flat surfaces only for GAG that had a low DS (Figures 1h and S14-S19 for CS-ODA ($DS_{0.12}$), Figures 1i and S20-S29 CS-PA ($DS_{0.25}$), Figure 2j and S35-S44 (HEP-ODA, $DS_{0.28}$), Figure 2k and S45-S52 (HEP-PA $DS_{0.15}$), and Figure 2l (HA-PA $DS_{0.12}$)). Indeed, the hexagonal shapes of NP obtained with high DS are not very well defined, the sides of the particles were not straight, and the typical sharp edges were not well identified (Figures 1g, 2i, S7-S13, S30-S34). One explanation is that the high DS results from a stronger interaction of the alkyl chains, making the interaction of the alkyl chains with the α-CD cavity difficult. Indeed, without α-CD, hydrophobically modified polysaccharides self-assemble into macromolecular micelles (Figure 1a-c and Figure 2a-d). The increase in the DS could result from compact inner cores of the macromolecular micelles, and, in turn, a lower interaction with α-CD is expected.

The analysis of electron microscopy images of NP obtained with low DS revealed that NP with a smaller size and narrower distribution were obtained with GAG hydrophobically modified with PA (Figures S53-S55 in the Supporting Information). Indeed, CS NP showed mean diameters measured

by TEM of 988.2 nm for CS-ODAm $DS_{0.28}$, and 333.3 nm for CS-PA, with a better uniformity distribution for CS-PA. Moreover, CS-PA NP showed hexagonal and flattened morphology. On the contrary, NP obtained with CS-ODAm $DS_{0.28}$ did not exhibit hexagonal and flattened morphology. HEP NP showed mean diameters measured by TEM of 631 nm for HEP-ODAm $DS_{0.28}$ and 187 nm for CS-PA, with a better uniformity distribution for HEP-PA.

Moreover, HEP-PA NP showed a hexagonal and well-formed flattened shape and NP, while particles obtained with HEP-ODAm $DS_{5.42}$ and HEP-ODAm $DS_{0.28}$ did not exhibit hexagonal morphology. Thus, HEP-PA showed the best blend between morphology, distribution uniformity, and mean diameter. Notably, the NP size could be optimized by prolonging the duration of mixing during NP preparation, as previously reported by Diaz-Salmeron et al.[15]

The zeta potentials of the suspensions of hydrophobically modified GAG in water and the NP were negative (Table 2a) in agreement with previous findings.[15, 17] Regardless of the GAG type, the DS, and the percentage of the α-CD, the zeta potentials were lower than -30 mV. The negative ζ of GAG preparations is due to the negative charge of carboxylate groups (of CS, HEP, and HA) and sulfate groups (for CS and HEP). In particular, the preparations composed of CS and HEP were strongly anionic compared with HA preparations. For the same alkyl chain, the NP composed of CS-PA had a zeta potential of -47.1 ± 2.0 mV, while the zeta potential of NP composed of HA-PA was ten-order of magnitude lower ($\zeta = -37.3 \pm 1.9$ mV). The zeta potential for all the GAG preparations was lower for NP than that for hydrophobically modified GAG suspensions in water. For example, the ζ for the suspension of CS-ODA ($DS_{5.42}$) was -37.0 ± 2.0 mV, and -44.3 ± 0.7 mV for CS-ODA NP. The decrease in the ζ could be due to the clustering of the GAG on the NP surface, compared with the suspension of hydrophobically modified GAG.

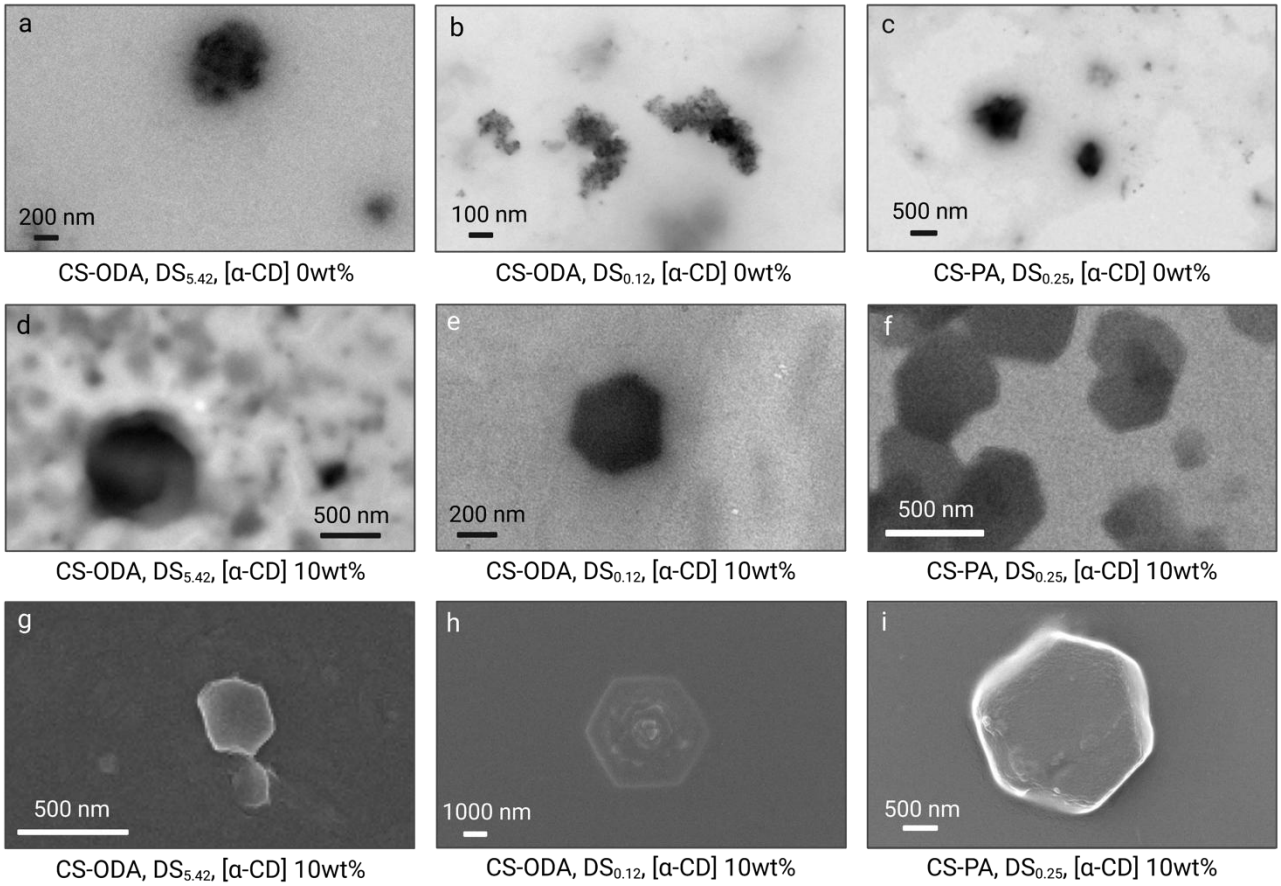

Figure 1. TEM and SEM pictures of particle suspensions obtained with CS-ODA and CS-PA. Hydrophobically modified CS were used at a concentration of (1 wt%) without α-CD or in the presence of α-CD at a concentration of 10 wt% in water. The suspensions were diluted in water (1/33) before observation.

Table 2. a) Zeta potentials (ζ) of hydrophobically modified polysaccharide suspensions and NP. Results are expressed as the mean ± SD (nm). Three measurements were performed for each formulation. b) IC_{30}, and c) IC_{50} values (μg mL^{-1}) at 24 h for GAG preparations after fitting to a dose-response curve in two different cell lines. All experiments were repeated three times. The IC_{50} and IC_{30} were obtained from Figures 3, 4, and S7 in the Supporting Information.

GAG preparation	DS_{NMR} (%)	α-CD wt%		a	b		c	
				ζ (mV) ± SD	IC_{30} (μg mL^{-1})		IC_{50} (μg mL^{-1})	
					J774A.1	HUCs	J774A.1	HUCs
CS	-	-	Solution	-	36	> 500	> 500	> 500
CS-ODA	5.42	0	Suspension	-37.0 ± 2.0	0.4	18	3.2	68
		10	NP	-44.3 ± 0.7	0.38	11	8.7	19
	0.12	0	Suspension	-31.4 ± 4.6	5	183	34.4	337.5
		10	NP	-40.2 ± 1.8	3.7	100	36.1	> 500
CS-PA	0.25	0	Suspension	-31.1 ± 5.8	39	>500	> 500	> 500
		10	NP	-47.1 ± 2.0	8.5	35	220.6	> 500
HEP	-	-	Solution	-	> 500	> 500	> 500	> 500
HEP-ODA	3.25	0	Suspension	-46.8 ± 1.6	0.6	24	1.9	38.7
		10	NP	-48.9 ± 0.2	0.4	3.6	1.4	7.13
	0.28	0	Suspension	-50.3 ± 3.0	2.1	78	56.3	> 500
		10	NP	-51.6 ± 1.5	1.4	27	36.1	191.3
HEP-PA	0.15	0	Suspension	-43.3 ± 1.1	94	> 500	202.5	> 500
		10	NP	-46.7 ± 3.3	16	115	50.5	> 500
HA	-	-	Solution	-	> 500	> 500	> 500	> 500
HA-PA	0.12	0	Suspension	-32.8 ± 2.6	27	333	459	> 500
		10	NP	-37.3 ± 1.9	21	70	245	447

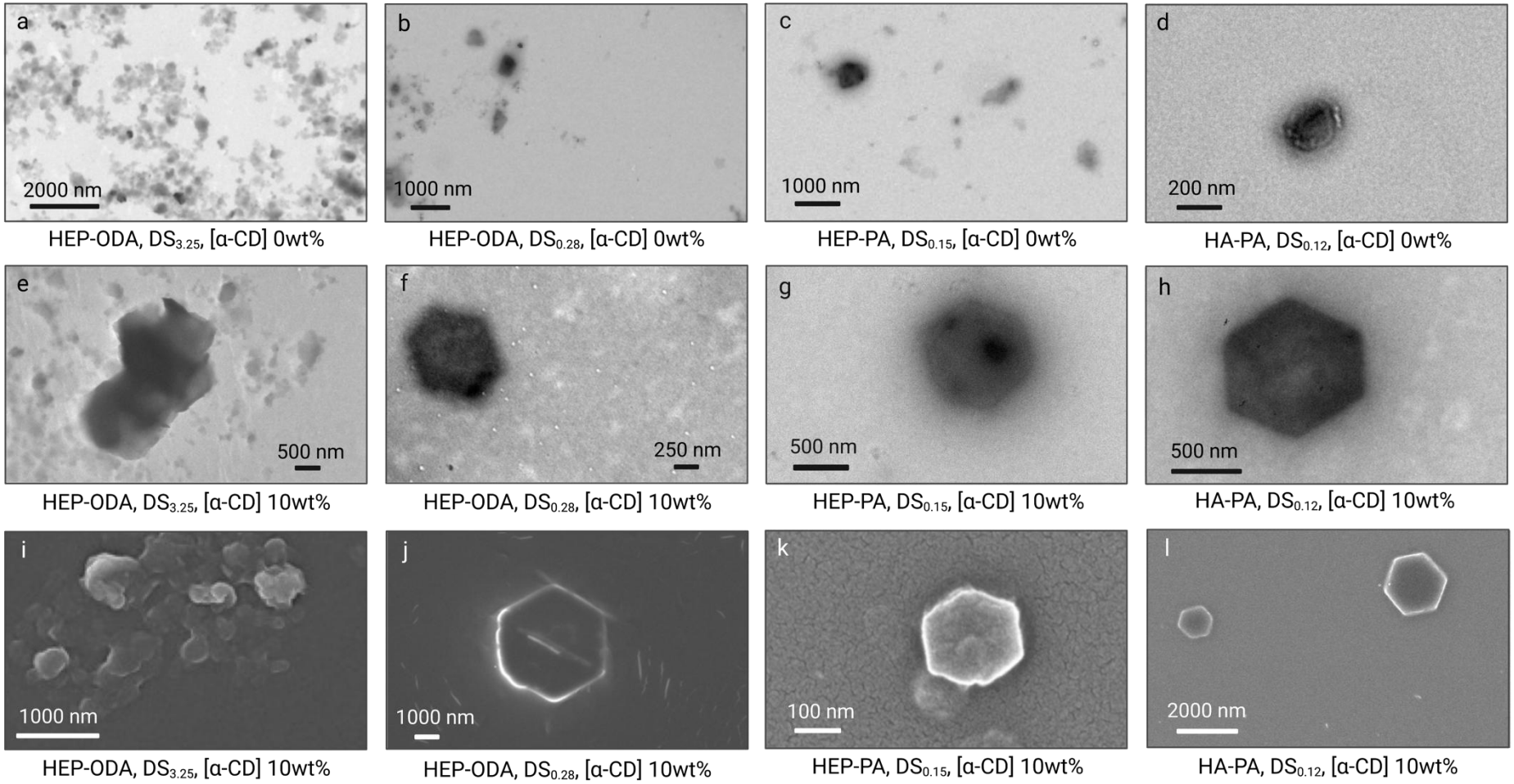

Figure 2. TEM and SEM pictures of particle suspensions obtained with HEP-ODA and HEP-PA. Hydrophobically modified HEP or HA were used at a concentration of (1 wt%) without α-CD or in the presence of α-CD at a concentration of 10 wt% in water. The suspensions were diluted in water (1/33) before observation.

4.3. In vitro evaluation of cytotoxicity

In this section, we performed cytotoxicity tests in two cell lines, macrophages, and human urothelial cells. Cytotoxicity tests were assessed by modifying the GAG type, the type of alkyl chain, and the DS. The cytotoxicity was evaluated for GAG solution, for suspensions of hydrophobically modified GAG, and for NP. The relative cell viability curves are presented in Figures 3, 4, and S59 (Supporting Information) for CS, HEP, and HA preparations, respectively. The values of the IC_{30} and IC_{50} are given in Table 2.b and 2.c, respectively. The results showed that the three GAG solutions were nontoxic in HUC in the tested concentration range ($0.01 - 500\ \mu g\ mL^{-1}$). However, the CS solution exhibited higher cytotoxicity in macrophages than HEP and HA. Indeed, the IC_{30} was reached at $36\ \mu g\ mL^{-1}$ of CS in macrophages (Table 2.b). The higher cytotoxicity in macrophages than in HUC could be due to the higher internalization of HA preparations. In addition to the non-specific phagocytosis function of macrophages, they naturally express hyaladherins receptors on their surface.[22] Unlike macrophages, the HUC do not have a phagocytosis function, and the CD44 expression on their surface is low.[23]

The covalent grafting of an alkyl chain on CS, HEP, and HA resulted in higher cytotoxicity, as observed from the cell viability curves and the IC_{30} values in Table 2.b. For example, the IC_{30} for HEP-ODA $DS_{3.25}$ was $0.6\ \mu g\ mL^{-1}$ in macrophages, while the HEP solution did not show any cytotoxic effect. Similarly, the IC_{30} of HEP-PA suspension was $94\ \mu g\ mL^{-1}$ in macrophages (Table 2.b). The higher cytotoxicity of the hydrophobically modified GAG than native GAG could be due to the higher interactions with the cell membrane. This hypothesis is confirmed by the higher cytotoxicity of hydrophobically modified GAG suspensions when the DS increases. Indeed, for each GAG type, the same grafting group, and the same cell line, the IC_{50} and the IC_{30} were lower when the DS increased. For example, the IC_{30} of CS-ODA suspension decreased from $4\ \mu g\ mL^{-1}$ to $0.4\ \mu g\ mL^{-1}$ in macrophages when the DS rosed from 0.12 to 5.42%.

The formulation of hydrophobically modified GAG as NP resulted from increased cytotoxicity in both cell lines. Higher cytotoxicity was reported for GAG NP than for hydrophobically modified GAG suspensions, probably because the higher negative charge condensed close to the cell membrane. Additionally, the flat morphology of the NP could result from higher interactions with the cell membrane,[24] and higher cell internalization.[13] Notably, the α-CD did not exhibit any cytotoxic effect (results not shown).

Regardless of the GAG type and the cell type, the hydrophobization by ODA resulted in higher cytotoxicity than the preparations grafted with PA. The IC_{50} in macrophages was six times lower for

NP composed of CS-ODA $DS_{0.12}$ than that of CS-PA $DS_{0.25}$ (Table 2.c). A similar tendency was observed for HEP NP. Those findings could be explained by the longer chain length for ODA (C18) than PA (C16). Indeed, previous data have shown that the toxicity increased with the alkyl chain length.[25] Previous works also demonstrated that functional groups play an essential role in inducing the toxicity of molecules containing alkyl chains. In particular, N-containing alkyl amines exhibited the highest cytotoxicity compared with other functional groups.[26] Finally, ODA is considered as a strong basic amine ($pKa = 10.6$). At the pH of the cytotoxicity experiments ($pKa = 7.4$), the ODA grafted on the GAG is cationic, resulting from higher cytotoxicity than nonionic and anionic compounds.[26]

According to the cytotoxicity results, the GAG, which are hydrophobically modified with PA were selected for the following experiments.

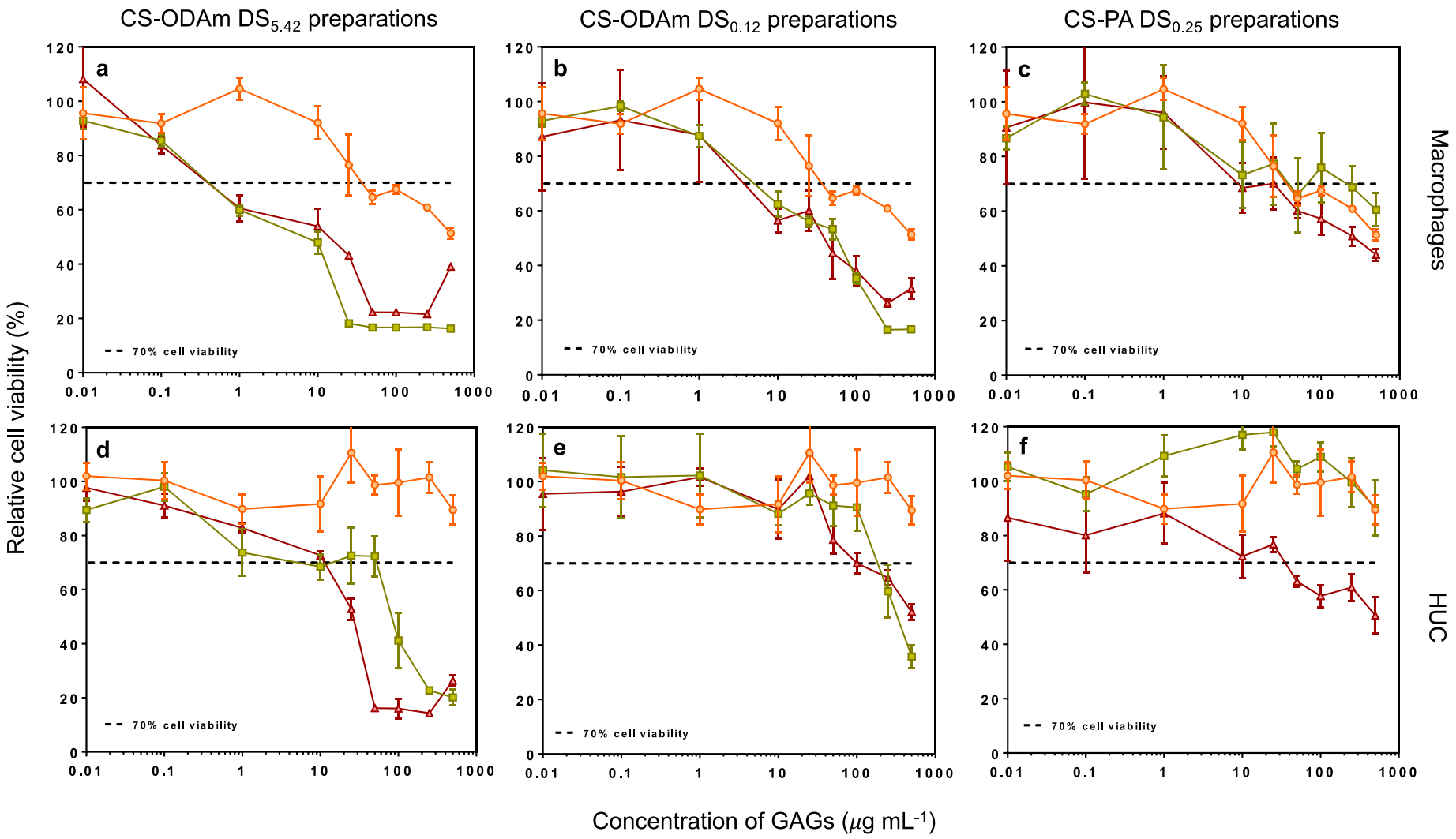

Figure 3. Cell viability testing of solutions of CS (circle, orange), hydrophobically modified CS suspensions (square, green), and CS NP (triangle, red). Dose-response data show the cytotoxicity to macrophages (a,b,c), and HUC (d,e,f). The two cell lines were exposed to different concentrations (0.01, 0.1, 1, 10, 25, 50, 100, 250, and 500 µg mL^{-1} of GAG. (a,d) CS-ODA $DS_{5.42}$, (b,e) CS-ODA $DS_{0.12}$, (c,f) CS-PA $DS_{0.25}$. The dotted lines show 70% of cell viability. Data are presented as the mean ± s.d. ($n = 6$ independent experiments).

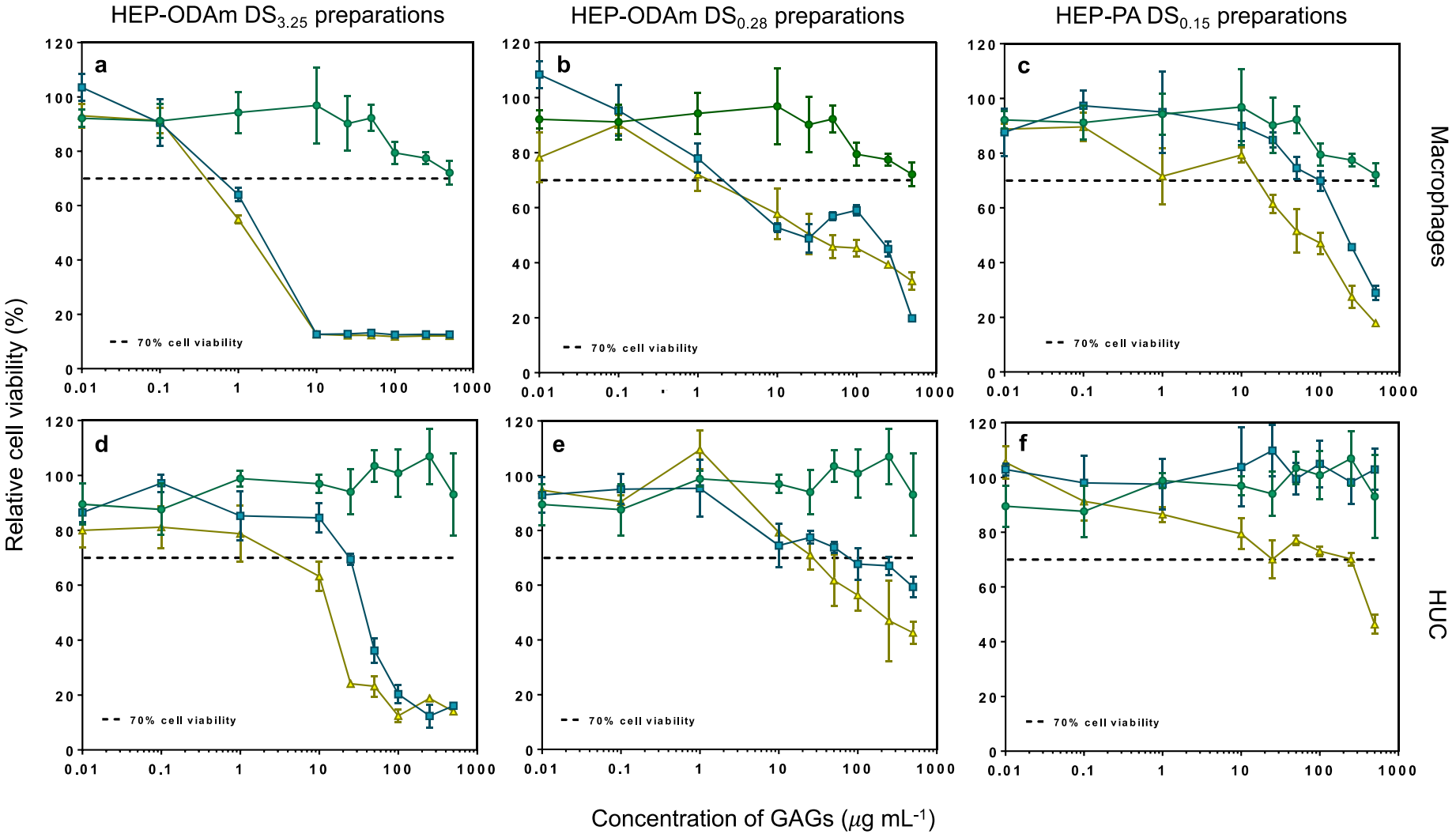

Figure 4. Cell viability testing of solutions of HEP (circle, dark green), hydrophobically modified HEP suspensions (square, dark turquoise blue), and HEP NP (triangle, light green). Dose-response data show the cytotoxicity to macrophages (a,b,c), and HUC (d,e,f). The two cell lines were exposed to different concentrations (0.01, 0.1, 1, 10, 25, 50, 100, 250, and 500 µg mL^{-1} of GAG. (a,d) HEP-ODA $DS_{3.25}$, (b,e) HEP-ODA $DS_{0.28}$, (c,f) HEP-PA $DS_{0.15}$. The dotted lines show 70% of cell viability. Data are presented as the mean ± s.d. ($n = 6$ independent experiments).

4.4. In vitro evaluation of the anti-inflammatory activity of GAG preparations

To evaluate the anti-inflammatory activity of GAG NP, the release of pro-inflammatory cytokine IL-6 by LPS-activated macrophages (denoted as LPS+ in Figure 5) was quantified after the cell exposition to NP suspensions. The NP suspensions were composed of CS-PA/α-CD, HEP-PA/α-CD, or HA-PA/α-CD (1/10 wt%). The GAG concentration was maintained at $25\ \mu g\ mL^{-1}$.

The results showed that HA NP induced a significant decrease in the IL-6 secretion (Figure 5, Panel a, Bar 3) compared with the untreated control (C1 in Figure 5). The anti-inflammatory activity of the HA NP was even higher than dexamethasone, used as a reference anti-inflammatory drug (C2 in Figure 5). NP composed of CS and HEP did not exhibit an anti-inflammatory activity (Figure 5, Panel b, Bar (6) and Figure 5, Panel c, Bar (9)). No significant differences in the IL-6 secretions were detected for CS NP and HEP NP compared with the IL-6 secretion in the untreated control. Similarly, no suppression of IL-6 secretion was reported with solutions of CS and HEP and suspensions of hydrophobically modified sulfated GAG (CS-PA and HEP-PA). Notably, as expected, low secretion of IL-6 was reported for macrophages without LPS treatment (denoted as LPS- in Figure 5).

To investigate the impact of the HA formulation on the anti-inflammatory activity, the IL-6 secretion induced upon macrophages incubation with HA NP, HA solution, or HA-PA suspension was quantified. Figure 5a revealed that the HA solution exhibited moderate anti-inflammatory activity, while HA-PA suspension and NP induced similar levels of IL-6 secretions. Those findings could be explained by the identical internalization rates of HA-PA and HA NP at a concentration of $25\ \mu g\ mL^{-1}$.[13] Indeed, the mechanism of the anti-inflammatory activity of HA requires its binding and internalization by macrophages. Internalization of HA-PA and HA NP was already demonstrated by confocal microscopy after 10 min of incubation.[13] Knowing that HA internalization by macrophages requires the cell surface receptor CD44,[27] previous results demonstrated that HA NP strongly interacted with recombinant human CD44 (rCD44).[13] The interaction of HA NP was higher than HA as a solution, as discussed earlier.[13]

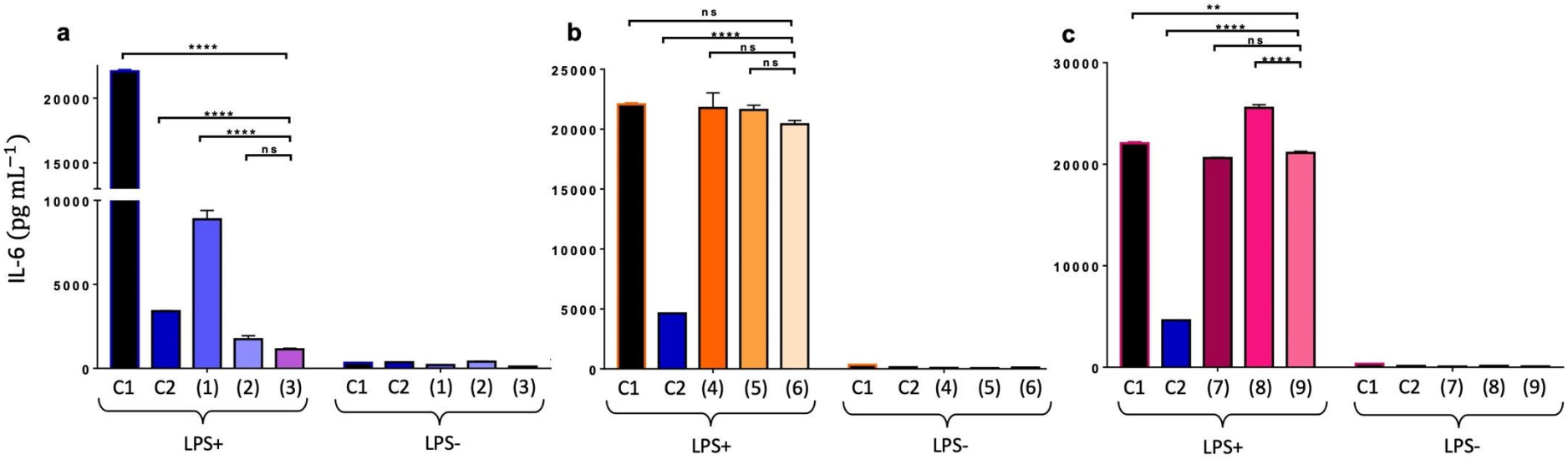

Figure 5. Concentration of IL-6 cytokine produced by macrophages with LPS induction (LPS+) or without LPS induction (LPS-) after treatment with preparations composed of HA (a), CS (b), and HEP (c). GAG were used at a concentration of 25 μg mL^{-1}. Samples treated with PBS were the positive controls of inflammation (C1). Dexamethasone was used as a reference anti-inflammatory drug (C2). GAG preparations were HA solution (1), HA-PA suspension (2), HA NP (3), CS solution (4), CS-PA suspension (5), CS NP (6), HEP solution (7), HEP-PA suspension (8) or HEP NP (9). One, two, three, and four asterisks denote *p*-values < 0.05; < 0.01; < 0.001 and < 0.0001 respectively, after one-way ANOVA followed by Tukey's multiple comparison post-test comparing the mean between different groups. No statistical significance was denoted by ns. Results are presented as mean ± SEM ($n = 3$ independent experiments).

4.5. In vivo anti-inflammatory activity in a BPS/IC rat model

In this section, the anti-inflammatory activities of NP composed of CS, HEP, and HA were evaluated after intravesical instillation to a rat model of LPS-induced inflammation. In this model, the inflammation was induced by the intravesical instillation of PS followed by the administration of LPS. After inducing the inflammation in the bladder, the Cy5.5 labeled preparations were administered to the living rats by intravesical instillation. The fluorescence signal was monitored after 24 h, 48 h, and 72 h of administration. Those durations were selected according to previous research investigations on HA NP performed on healthy rats.[28] Herein, the inflammation induced in the rat bladder could modify NP distribution and bioelimination. Indeed, the residence time of the GAG formulations inside the healthy bladder differed from that of the inflamed bladder.[29] High-resolution scan images of inflamed rat bladder mucosa highlighted significant changes compared with healthy, noninflamed mucosa (Figure 6a,b). As expected, healthy bladders did not show any sign of inflammatory infiltration. Few immune cells (macrophages) were observed in the bladder tissue, mainly in lamina propria. There were no urothelial degeneration and significant arterial dilatation (Figure 6a,b). The inflamed bladder mucosa is characterized by a loss of the urothelium, the presence of edema, and leucocyte infiltration (Figure 6c, d). The structure of the lamina propria and the smooth muscle cell layer was altered compared to high-resolution scan images of a healthy bladder. Several disorders were reported with inflamed bladders, including increased mucosal permeability and inflammatory cell infiltration in the urothelium and the lamina propria.[30] Inflammation recruits immune cells and macrophages, a source of pro-inflammatory cytokines.

Real-time fluorescence images in Figure 7 showed that HA NP had the highest fluorescence signal compared with CS NP and HEP NP after 24 h, 48 h, and 72 h. The fluorescence signal of HA NP in the inflamed bladder was in the same range as that observed for the noninflamed bladder (see Figure 5 in our previous work).[28] Higher residence time of HA NP compared with CS NP and HEP NP could be due to the higher interaction of HA NP with the urothelial cells and macrophages. To test this hypothesis, the same experiment was conducted with solutions of GAG. The results in Figure 7 showed that HA solution exhibited a higher fluorescence signal at 24 h postadministration than solutions of CS and HEP. However, this fluorescence signal of the HA solution rapidly decreased at 48 h postadministration and reached the same range as CS and HEP solution. Regardless of the GAG type, their formulation as NP increased their bioaccumulation in the bladder compared with a solution of GAG and to suspensions of hydrophobically modified GAG (Figure 7). This increase could be due to the flattened morphology of the GAG NP, which results in higher surface contact with the urothelium, improving thus the bioaccumulation in the bladder. Several research works revealed that the nonspherical morphology of nanoparticles resulted in multivalent

interactions with the cell surface increasing the rate and the strength of attachment to the cell membrane.

The therapeutic efficacy of the GAG preparations was then evaluated *in vivo* 72 h postadministration by histopathological analysis of the bladder mucosa. An inflammation score was attributed to each group to estimate the degree of bladder damage.[31] The high-resolution scan images of the bladder sections treated with HA preparations are shown in Figure 6e-j. The histological images of bladder sections treated with CS and HEP preparations are shown in the Supplementary Information (Figures S60 and S61).

Rats treated with an HA solution presented a decrease in the inflammation signs (Figure 6e,f). There were no micro-abscesses corresponding to the accumulation of polymorphonuclear neutrophils (PMN), and the urothelial damage was decreased significantly. A decrease in the global inflammation score was reported in Figure 8a, compared with the untreated group. A decrease in venous congestion, edema, cell infiltration, and urothelial damage was reported in the histological score (Figure 8a'). Similar observations were reported for CS, and HEP solutions since a decrease in the global inflammation score (Figure 8b,c) and the histological score (Figure 8b',c') were reported. The reduction in the global inflammation score after GAG administration is expected because the intrinsic anti-inflammatory activity of HA, CS, and HEP was already demonstrated.[32] The mechanism of the GAG anti-inflammatory activity involves CD44[33] and Toll-like receptors (TLRs).[34] Among the three GAG explored in this investigation, most of the data in the literature were focused on the anti-inflammatory mechanism of HA. HA is able to inhibit and down-regulate the expression and protein synthesis of IL-1β,[35] IL-6,[35, 36] IL-8,[37] NO, or TNF-α.[36] HA also inhibits mast cell degranulation,[38] while the activation of mast cell degranulation is a crucial step in the pathogenesis of BPS/IC.[39] However, in this investigation, we revealed that the reduction in the inflammation after HA administration in inflamed rat bladder was moderate since mild edema and veinous congestion were still present in the lamina propria. We could also observe some fields with hemorrhage for HA solution (Figure 6e,f).

Rats treated with HA-PA suspension presented a slight decrease in histological signs of inflammation compared with the untreated group. Venous congestion, edema, cell infiltration, and urothelial damage were decreased in the group treated with HA-PA compared with the untreated group (Figure 8a'). However, the global inflammation score of the group treated with HA-PA was non significantly different from the group treated with HA (Figure 8a), and the urothelial damage slightly increased with HA-PA suspension. Moderate edema, cellular infiltration, and venous congestion were still present, as observed from the high-resolution scan images in Figure 6e,f. Similar observations were reported for hydrophobically modified CS and HEP compared with solutions of native sulfated GAG (Figure 8b,c and Figure 8b',c').

Interestingly, the formulation of HA-PA suspensions as NP resulted in a strong and statistically significant decrease in the global inflammation score compared with the bladders of rats treated with HA solution and HA-PA suspension. A similar tendency was observed in the histological scan images of bladders treated with CS NP and HEP NP. Regardless of the GAG type, their formulation as NP induced a decrease in venous congestion, edema, PMN infiltration, and urothelial damage (Figure 8a',b',c'). A better reduction in inflammation signs observed with GAG NP than GAG in solution is due to the typical properties of those NP. Collected data from the literature showed that the typical NP morphology, the organization of the GAG on their surface, and their low Young's modulus impact several behaviors.[13, 28, 40] In comparison with spherical particles, the NP had faster diffusion in water. The surface explored by the NP was higher than that explored by a spherical particle.[40] The morphology-dependent self-motion of the NP could increase particle transport inside the bladder cavity to reach the urothelium surface. The bioadhesion kinetics studied ex vivo showed that HA NP reached the urothelium rapidly and remained firmly attached to the bladder.[28] Notably, the HA itself showed low bioadhesive behaviors.[28]

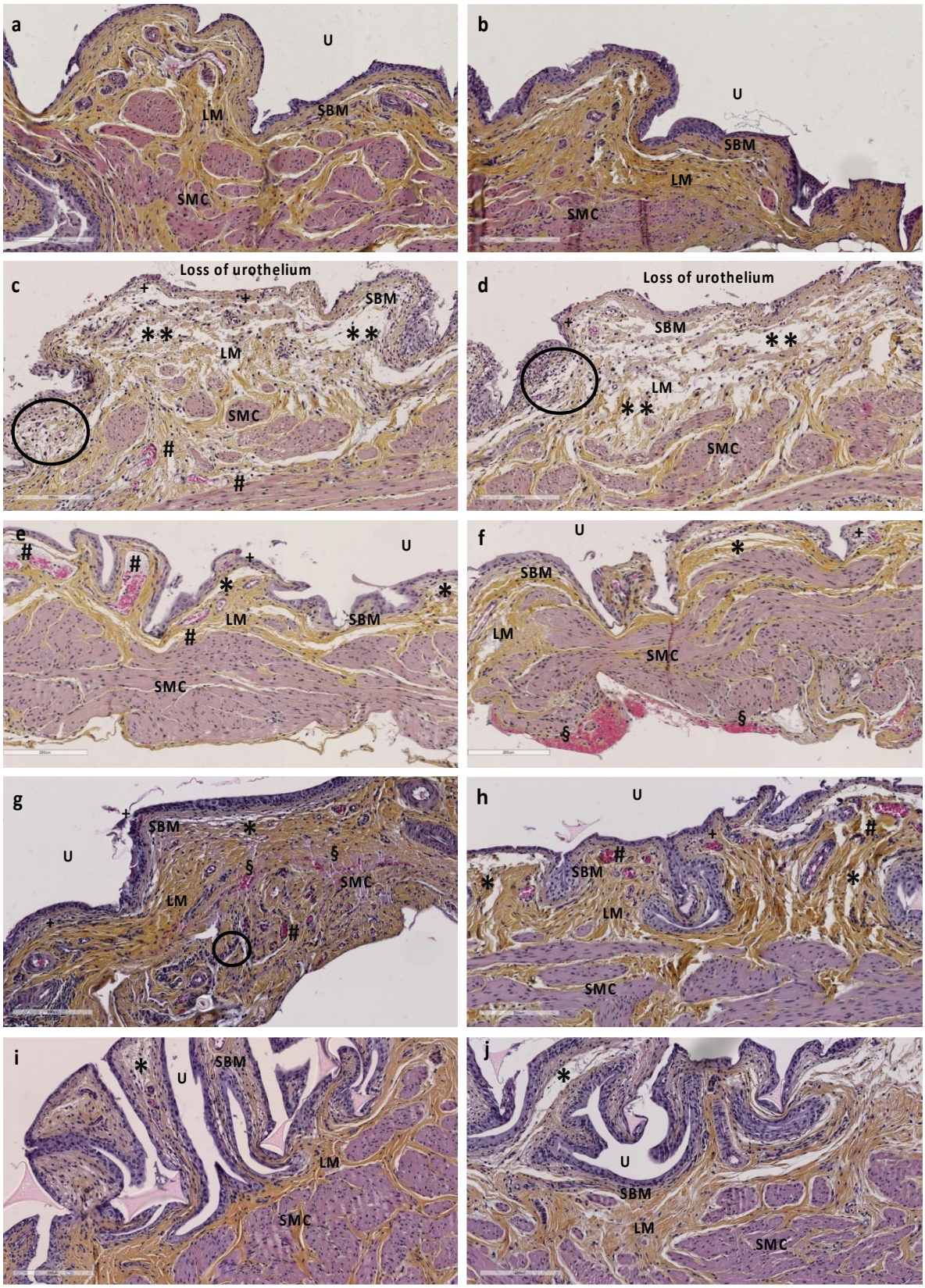

Figure 6. HES-stained high-resolution scans of bladders collected from healthy rats (a,b) or from rats after intravesical instillation of LPS/PS (c,d). HA preparations were administered as HA solution (e,f), HA-PA suspension (g,h), or HA NP (i,j) at a concentration of 10 mg mL^{-1} in HA. # veinous congestion. *Circles*, leucocytes infiltration. *§*, hemorrhage. +, urothelial thinning or ulceration. *, mild edema. **, moderate edema. *U*, urothelium. *SBM*, submucosa. *LM*, lamina propria. *SMC*, smooth muscle cell layer. The scale bar represents 200 µm

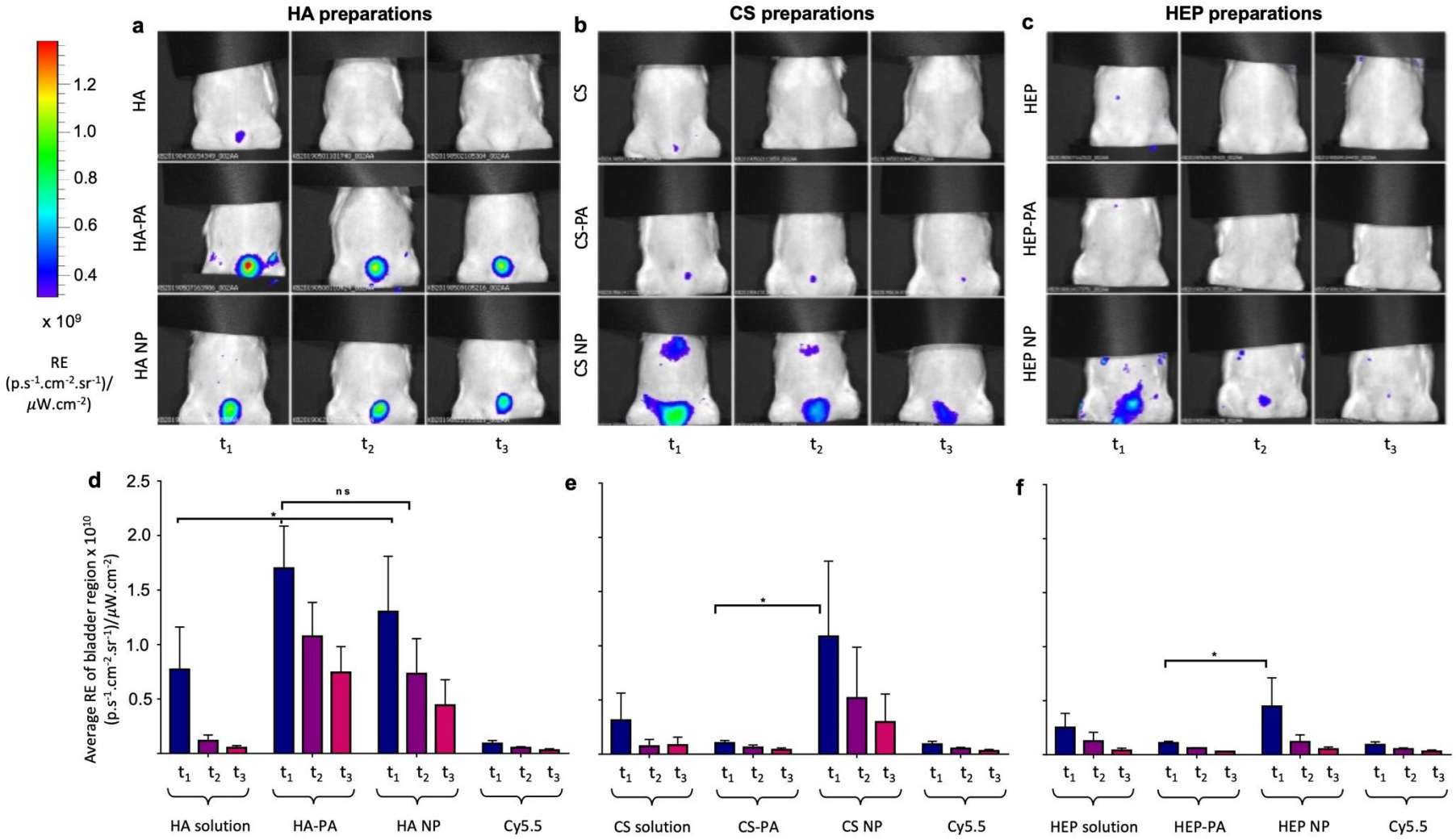

Figure 7. (a,b,c) IVIS Lumina scans and (d,e,f) average radiant efficiency (RE) of rat abdomens after 24 h (t_1), 48 h (t_2), and 72 h (t_3) postadministration of preparations composed of HA (a,d), CS (b,e) and HEP (c,f). GAG preparations were HA solution (1), HA-PA suspension (2), HA NP (3), CS solution (4), CS-PA suspension (5), CS NP (6), HEP solution (7), HEP-PA suspension (8) or HEP NP (9). GAG were used at a concentration of 10 mg mL^{-1}. Rats treated with a solution of Cy5.5, are used as a control (C). One asterisk denoted p-value < 0.05 after two-way Kruskal-Wallis test followed by a Tukey's multiple comparison post-test. $n = 3$ rats for each group.

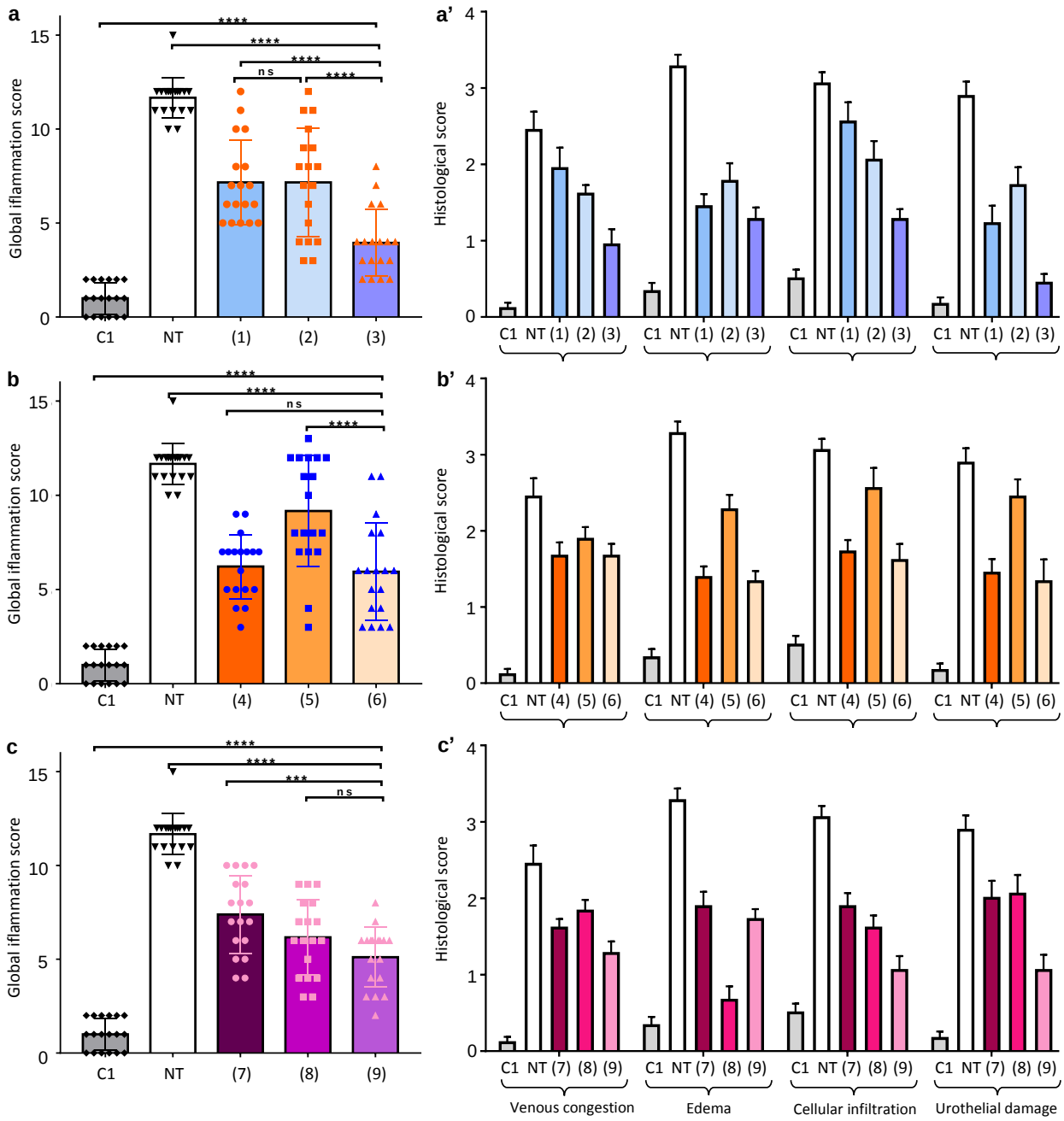

Figure 8. (a,b,c) Global inflammation scores obtained from the analysis of high-resolution scan images of the bladder inflammation 72 h postadministration of preparations composed of HA (a), CS (b), or HEP (c). GAG preparations were HA solution (1), HA-PA suspension (2), HA NP (3), CS solution (4), CS-PA suspension (5), CS NP (6), HEP solution (7), HEP-PA suspension (8) or HEP NP (9). C1 represents the healthy rat group, and NT represents the non-treated rat group in which the inflammation was induced. Tissues were scored from 0 to 4 for venous congestion, edema, cellular infiltration, and urothelial damage (a',b',c'), giving a maximal histological score of 16 per slide. Statistical analysis was performed with two-way ANOVA followed by Tukey's post-test. One, two, three, and four asterisks denoted *p*-value < 0.05, < 0.01, < 0.001, and < 0.0001, respectively. No significant differences were denoted by ns. $n = 3$ rats for each group, and 6 images for each group were analyzed.

5. Conclusion

In summary, in this investigation, we reported that the formulation of GAG as NP that have a typical flattened morphology could be used as an efficient GAG replenishment therapy to alleviate BPS/IC. Herein, we demonstrated that the intrinsic anti-inflammatory activity of the GAG NP was higher than a solution of GAG in a rat model of BPS/IC. The higher activity of the GAG NP compared with solutions of GAG could result from several events. Indeed, due to their flattened morphology, the GAG NP can rapidly diffuse in a diluted fluid.[12] When the NP reached the bladder mucosa, they rapidly adhered to the urothelium at low concentrations.[41] The interaction with the urothelial cells occurs through receptor-mediated multivalent binding.[13] Consequently, the residence time of the GAG NP in the bladder was prolonged, resulting in better anti-inflammatory activity than native GAG. Those findings could be interesting for clinical use because the prolonged residence time of the GAG NP in the bladder results in higher biological activity and a reduction in the frequency of the administration of the formulations in the bladder. Notably, the long-term beneficial effect of the instillation of a GAG solution in the bladder was observed in only two-thirds of patients.[42] The second major conclusion of this work is that, among the three GAG used in this investigation, HA NP exhibited the best decrease in urothelial bladder inflammation and allowed regeneration of the urothelial surface. This therapeutic strategy could be a good alternative to the market treatment consisting of the instillation of a HA solution in the bladder. Future investigations will be focused on studying the eventual synergistic activity between the HA NP and an anti-inflammatory drug.

6. Funding

This work was supported by the Institut Universitaire de France, the ANR-17-CE09-0038 and ANR-21-CE09-0015.

7. Acknowledgements

The present work has benefited from the Imagerie- Gif core facility supported by l'Agence Nationale de la Recherche (ANR-11-EQPX-0029/Morphoscope, ANR-10-INBS-04/FranceBioImaging; ANR- 11- IDEX- 0003- 02/Saclay Plant Sciences). We are thankful to Rémy Pires Brazuna for his technical assistance in the SEM observations and the electron microscopy facilities from the Institut de Chimie et des Matériaux Paris-Est (ICMPE), UMR 7182 CNRS-Université Paris Est Créteil, 94320, Thiais, France. Raul Diaz-Salmeron was supported by the French Ministère de l'Enseignement Supérieur et de la Recherche (MESR).

8. References

(1) Dobberfuhl, A. D. Pathophysiology, assessment, and treatment of overactive bladder symptoms in patients with interstitial cystitis/bladder pain syndrome. *Neurourology and Urodynamics* **2022**, *41* (8), 1958-1966. Yu, W.-R.; Chang, W.-C.; Kuo, H.-C. Clinical presentation, videourodynamic characteristics, and treatment outcome in men with interstitial cystitis-like lower urinary tract symptoms. *International Urology and Nephrology* **2022**, *54* (9), 2157-2165.
(2) Moore, K. H. Interstitial Cystitis. In *Urogynecology: Evidence-Based Clinical Practice*, Springer, 2022; pp 229-236.
(3) Parsons, C. A model for the function of glycosaminoglycans in the urinary tract. *World journal of urology* **1994**, *12* (1), 38-42.
(4) Parsons, L.; Boychuk, D.; Jones, S.; Hurst, R.; Callahan, H. Bladder surface glycosaminoglycans: an epithelial permeability barrier. *The Journal of urology* **1990**, *143* (1), 139-142.
(5) Janssen, D. A.; van Wijk, X. M.; Jansen, K. C.; van Kuppevelt, T. H.; Heesakkers, J. P.; Schalken, J. A. The distribution and function of chondroitin sulfate and other sulfated glycosaminoglycans in the human bladder and their contribution to the protective bladder barrier. *The Journal of urology* **2013**, *189* (1), 336-342.
(6) Erickson, D. R.; Xie, S. X.; Bhavanandan, V. P.; Wheeler, M. A.; Hurst, R. E.; Demers, L. M.; Kushner, L.; Keay, S. K. A comparison of multiple urine markers for interstitial cystitis. *The Journal of urology* **2002**, *167* (6), 2461-2469. Erickson, D. R.; Belchis, D. A.; Dabbs, D. J. Inflammatory cell types and clinical features of interstitial cystitis. *The Journal of urology* **1997**, *158* (3), 790-793.
(7) Wyndaele, J. J. J.; Riedl, C.; Taneja, R.; Lovász, S.; Ueda, T.; Cervigni, M. GAG replenishment therapy for bladder pain syndrome/interstitial cystitis. *Neurourology and urodynamics* **2019**, *38* (2), 535-544. Cervigni, M. Interstitial cystitis/bladder pain syndrome and glycosaminoglycans replacement therapy. *Translational andrology and urology* **2015**, *4* (6), 638.
(8) Nickel, J. C.; Tripp, D. A.; Pontari, M.; Moldwin, R.; Mayer, R.; Carr, L. K.; Doggweiler, R.; Yang, C. C.; Mishra, N.; Nordling, J. Interstitial cystitis/painful bladder syndrome and associated medical conditions with an emphasis on irritable bowel syndrome, fibromyalgia and chronic fatigue syndrome. *The Journal of urology* **2010**, *184* (4), 1358-1363. Moldwin, R. M.; Evans, R. J.; Stanford, E. J.; Rosenberg, M. T. Rational approaches to the treatment of patients with interstitial cystitis. *Urology* **2007**, *69* (4), S73-S81. Kallestrup, E. B.; Jørgensen, S. S.; Nordling, J.; Hald, T. Treatment of interstitial cystitis with Cystistat®, A hyaluronic acid product. *Scandinavian journal of urology and nephrology* **2005**, *39* (2), 143-147.
(9) Kuo, H. Urodynamic results of intravesical heparin therapy for women with frequency urgency syndrome and interstitial cystitis. *Journal of the Formosan Medical Association* **2001**, *100* (5), 309-314. Parsons, C.; Housley, T.; Schmidt, J.; Lebow, D. Treatment of interstitial cystitis with intravesical heparin. *British Journal of Urology* **1994**, *73* (5), 504-507. Porru, D.; Leva, F.; Parmigiani, A.; Barletta, D.; Choussos, D.; Gardella, B.; Daccò, M. D.; Nappi, R. E.; Allegri, M.; Tinelli, C. Impact of intravesical hyaluronic acid and chondroitin sulfate on bladder pain syndrome/interstitial cystitis. *International urogynecology journal* **2012**, *23* (9), 1193-1199.
(10) Tyagi, P.; Wu, P.-C.; Chancellor, M.; Yoshimura, N.; Huang, L. Recent advances in intravesical drug/gene delivery. *Molecular pharmaceutics* **2006**, *3* (4), 369-379. Tyagi, P.; Li, Z.; Chancellor, M.; De Groat, W. C.; Yoshimura, N.; Huang, L. Sustained intravesical drug delivery using thermosensitive hydrogel. *Pharmaceutical research* **2004**, *21* (5), 832-837. GuhaSarkar, S.; More, P.; Banerjee, R. Urothelium-adherent, ion-triggered liposome-in-gel system as a platform for intravesical drug delivery. *Journal of Controlled Release* **2017**, *245*, 147-156. GuhaSarkar, S.; Banerjee, R. Intravesical drug delivery: challenges, current status, opportunities and novel strategies. *Journal of Controlled Release* **2010**, *148* (2), 147-159.
(11) Ahmed, Z.; Malli, S.; Diaz-Salmeron, R.; Destruel, P.-L.; Da Costa, A.; Guigner, J.-M.; Porcher, F.; Baptiste, B.; Ponchel, G.; Bouchemal, K. New insights on the structure of hexagonally faceted platelets from hydrophobically modified chitosan and α-cyclodextrin. *International Journal of Pharmaceutics* **2018**, *548* (1), 23-33. DOI: 10.1016/j.ijpharm.2018.06.035.

(12) Diaz-Salmeron, R.; Da Costa, A.; Michel, J.-P.; Ponchel, G.; Bouchemal, K. Real-Time Visualization of Morphology-Dependent Self-Motion of Hyaluronic Acid Nanomaterials in Water. *International Journal of Pharmaceutics* **2021**, 121172. DOI: https://doi.org/10.1016/j.ijpharm.2021.121172.
(13) Diaz-Salmeron, R.; Michel, J.-P.; Hadji, H.; Gout, E.; Vivès, R. R.; Ponchel, G.; Bouchemal, K. Role of the interactions with CD44 and supported bilayer membranes in the cellular uptake of soft multivalent hyaluronan nanoparticles. *Colloids and Surfaces B: Biointerfaces* **2021**, 111916.
(14) Diaz-Salmeron, R.; Toussaint, B.; Cailleau, C.; Ponchel, G.; Bouchemal, K. Morphology-Dependent Bioadhesion and Bioelimination of Hyaluronan Particles Administered in the Bladder. *Advanced NanoBiomed research* **2022**, 2100138. DOI: 10.1002/anbr.202100138.
(15) Diaz-Salmeron, R.; Ponchel, G.; Bouchemal, K. Hierarchically built hyaluronan nano-platelets have symmetrical hexagonal shape, flattened surfaces and controlled size. *European Journal of Pharmaceutical Sciences* **2019**, *133*, 251-263. DOI: 10.1016/j.ejps.2019.04.007.
(16) Galus, A.; Mallet, J.-M.; Lembo, D.; Cagno, V.; Djabourov, M.; Lortat-Jacob, H.; Bouchemal, K. Hexagonal-shaped chondroitin sulfate self-assemblies have exalted anti-HSV-2 activity. *Carbohydrate Polymers* **2016**, *136*, 113-120.
(17) Lembo, D.; Donalisio, M.; Laine, C.; Cagno, V.; Civra, A.; Bianchini, E. P.; Zeghbib, N.; Bouchemal, K. Auto-associative heparin nanoassemblies: a biomimetic platform against the heparan sulfate-dependent viruses HSV-1, HSV-2, HPV-16 and RSV. *European Journal of Pharmaceutics and Biopharmaceutics* **2014**, *88* (1), 275-282.
(18) Diaz-Salmeron, R.; Ponchel, G.; Gallard, J.-F.; Bouchemal, K. Hierarchical supramolecular platelets from hydrophobically-modified polysaccharides and α-cyclodextrin: Effect of hydrophobization and α-cyclodextrin concentration on platelet formation. *International Journal of Pharmaceutics* **2018**, *548* (1), 227-236.
(19) Grisin, T.; Bories, C.; Bombardi, M.; Loiseau, P. M.; Rouffiac, V.; Solgadi, A.; Mallet, J.-M.; Ponchel, G.; Bouchemal, K. Supramolecular chitosan micro-platelets synergistically enhance anti-*Candida albicans* activity of amphotericin B using an immunocompetent murine model. *Pharmaceutical Research* **2017**, *34* (5), 1067-1082. Grisin, T.; Bories, C.; Loiseau, P. M.; Bouchemal, K. Cyclodextrin-mediated self-associating chitosan micro-platelets act as a drug booster against *Candida glabrata* mucosal infection in immunocompetent mice. *International Journal of Pharmaceutics* **2017**, *519* (1-2), 381-389. DOI: doi.org/10.1016/j.ijpharm.2017.01.048.
(20) Palumbo, F. S.; Pitarresi, G.; Mandracchia, D.; Tripodo, G.; Giammona, G. New graft copolymers of hyaluronic acid and polylactic acid: Synthesis and characterization. *Carbohydrate polymers* **2006**, *66* (3), 379-385.
(21) Carn, F.; Nowak, S.; Chaab, I.; Diaz-Salmeron, R.; Djabourov, M.; Bouchemal, K. Autoassemblies of α-cyclodextrin and grafted polysaccharides: Crystal structure and specific properties of the platelets. *The Journal of Physical Chemistry B* **2018**, *122* (22), 6055-6063.
(22) Gustafson, S.; Forsberg, N. Hyaluronan-binding proteins on cultured J 774 macrophages. *Biochimica et Biophysica Acta (BBA)-Molecular Cell Research* **1991**, *1091* (1), 36-40.
(23) Au, Y. M. Involvement of CD44 during tumorigenic transformation of pre-cancerous human uroepithelial cells. **2012**.
(24) Hadji, H.; Bouchemal, K. Effect of micro- and nanoparticle shape on biological processes. *Journal of Controlled Release* **2022**, *342*, 93-110. DOI: https://doi.org/10.1016/j.jconrel.2021.12.032.
(25) Liu, W.; Wang, X.; Zhou, X.; Duan, H.; Zhao, P.; Liu, W. Quantitative structure-activity relationship between the toxicity of amine surfactant and its molecular structure. *Science of the Total Environment* **2020**, *702*, 134593.
(26) Versteeg, D. J.; Stanton, D. T.; Pence, M. A.; Cowan, C. Effects of surfactants on the rotifer, Brachionus calyciflorus, in a chronic toxicity test and in the development of QSARs. *Environmental Toxicology and Chemistry: An International Journal* **1997**, *16* (5), 1051-1058.
(27) Culty, M.; Nguyen, H. A.; Underhill, C. B. The hyaluronan receptor (CD44) participates in the uptake and degradation of hyaluronan. *The Journal of cell biology* **1992**, *116* (4), 1055-1062.
(28) Diaz-Salmeron, R.; Toussaint, B.; Cailleau, C.; Ponchel, G.; Bouchemal, K. Morphology-Dependent Bioadhesion and Bioelimination of Hyaluronan Particles Administered in the Bladder. *Advanced NanoBiomed Research* **2022**, *2* (5), 2100138.

(29) Hauser, P. J.; Buethe, D. A.; Califano, J.; Sofinowski, T. M.; Culkin, D. J.; Hurst, R. E. Restoring barrier function to acid damaged bladder by intravesical chondroitin sulfate. *The Journal of urology* **2009**, *182* (5), 2477-2482.
(30) Johansson, S. L.; Fall, M. Clinical features and spectrum of light microscopic changes in interstitial cystitis. *The Journal of urology* **1990**, *143* (6), 1118-1124. Skoluda, D.; Richter, I.-E.; Busse, K. Experiments in coli cystitis. *Urologia Internationalis* **1974**, *29* (4), 299-311.
(31) Oottamasathien, S.; Jia, W.; McCoard, L.; Slack, S.; Zhang, J.; Skardal, A.; Job, K.; Kennedy, T. P.; Dull, R. O.; Prestwich, G. D. A murine model of inflammatory bladder disease: cathelicidin peptide induced bladder inflammation and treatment with sulfated polysaccharides. *The Journal of urology* **2011**, *186* (4S), 1684-1692.
(32) Iovu, M.; Dumais, G.; Du Souich, P. Anti-inflammatory activity of chondroitin sulfate. *Osteoarthritis and Cartilage* **2008**, *16*, S14-S18. Ronca, F.; Palmieri, L.; Panicucci, P.; Ronca, G. Anti-inflammatory activity of chondroitin sulfate. *Osteoarthritis and Cartilage* **1998**, *6*, 14-21.
(33) Teder, P.; Vandivier, R. W.; Jiang, D.; Liang, J.; Cohn, L.; Puré, E.; Henson, P. M.; Noble, P. W. Resolution of lung inflammation by CD44. *Science* **2002**, *296* (5565), 155-158. Zhao, G.; Shaik, R. S.; Zhao, H.; Beagle, J.; Kuo, S.; Hales, C. A. Low molecular weight (LMW) heparin inhibits injury-induced femoral artery remodeling in mouse via upregulating CD44 expression. *Journal of vascular surgery* **2011**, *53* (5), 1359-1367. e1353.
(34) You, N.; Chu, S.; Cai, B.; Gao, Y.; Hui, M.; Zhu, J.; Wang, M. Bioactive hyaluronic acid fragments inhibit lipopolysaccharide-induced inflammatory responses via the Toll-like receptor 4 signaling pathway. *Frontiers of Medicine* **2021**, *15* (2), 292-301.
(35) Hee, C. K.; Messina, D. J. In vitro inflammatory and immune response to uncrosslinked hyaluronic acid (HA) and HA fillers. *Journal of Immunology and Regenerative Medicine* **2022**, *17*, 100065.
(36) Zheng, B. W.; Wang, B. Y.; Xiao, W. L.; Sun, Y. J.; Yang, C.; Zhao, B. T. Different molecular weight hyaluronic acid alleviates inflammation response in DNFB-induced mice atopic dermatitis and LPS-induced RAW 264.7 cells. *Life Sciences* **2022**, *301*, 120591.
(37) Stellavato, A.; Pirozzi, A. V. A.; Diana, P.; Reale, S.; Vassallo, V.; Fusco, A.; Donnarumma, G.; De Rosa, M.; Schiraldi, C. Hyaluronic acid and chondroitin sulfate, alone or in combination, efficiently counteract induced bladder cell damage and inflammation. *PLoS One* **2019**, *14* (6), e0218475.
(38) Boucher, W.; Letourneau, R.; Huang, M.; Kempuraj, D.; Green, M.; Sant, G.; Theoharides, T. Intravesical sodium hyaluronate inhibits the rat urinary mast cell mediator increase triggered by acute immobilization stress. *The Journal of urology* **2002**, *167* (1), 380-384.
(39) Wen, C.; Xie, L.; Hu, C. Roles of mesenchymal stem cells and exosomes in interstitial cystitis/bladder pain syndrome. *Journal of Cellular and Molecular Medicine* **2022**, *26* (3), 624-635.
(40) Diaz-Salmeron, R.; Da Costa, A.; Michel, J.-P.; Ponchel, G.; Bouchemal, K. Real-time visualization of morphology-dependent self-motion of hyaluronic acid nanomaterials in water. *International Journal of Pharmaceutics* **2021**, *609*, 121172.
(41) Diaz-Salmeron, R.; Toussaint, B.; Cailleau, C.; Ponchel, G.; Bouchemal, K. Morphology-Dependent Bioadhesion and Bioelimination of Hyaluronan Particles Administered in the Bladder. *Advanced NanoBiomed Research* **2022**, 2100138.
(42) Nordling, J.; Jørgensen, S.; Kallestrup, E. Cystistat for the treatment of interstitial cystitis: a 3-year follow-up study. *Urology* **2001**, *57* (6), 123.

Separate Figures and Tables

Table 1. Degrees of substitutions of different hydrophobically-modify compounds were calculated by elemental analysis (DS_{EA}) and ^{1}H-NMR (DS_{NMR}).

Sample	C mol%	H mol%	N mol%	O mol%	S mol%	C/S mol%	C/O mol%	DS_{EA}* (%)	**DS_{NMR} (%)
CS	2.38	4.89	0.24	3.10	0.13	17.92	0.77	-	-
CS-ODA DS_{High}	3.11	6.37	0.35	2.58	0.13	25.40	1.21	6.55	5.42
CS-ODA DS_{Low}	2.88	5.84	0.38	2.81	0.15	18.09	1.02	0.15	0.12
CS-PA	2.45	5.00	0.20	3.02	0.13	18.21	0.81	0.22	0.25
HEP	1.76	3.86	0.13	2.97	0.25	7.07	0.59	-	-
HEP-ODA DS_{High}	2.89	6.15	0.30	2.55	0.24	12.25	1.13	4.53	3.25
HEP-ODA DS_{Low}	2.14	4.49	0.24	2.97	0.28	7.44	0.72	0.31	0.28
HEP-PA	1.9	4.05	0.14	3.08	0.26	7.33	0.62	0.20	0.15
HA	6.07	5.68	0.44	6.09	0	-	1.00	-	-
HA-PA	6.33	5.94	0.60	5.55	0	-	1.14	0.14	0.12

*Equation S1 for sulfated GAG and Equation S2 for HA in the Supporting Information.
**DS calculated from ^{1}H NMR by integrating the characteristic signals of alkyl chain protons[20] in Figure S6 in the Supporting Information.

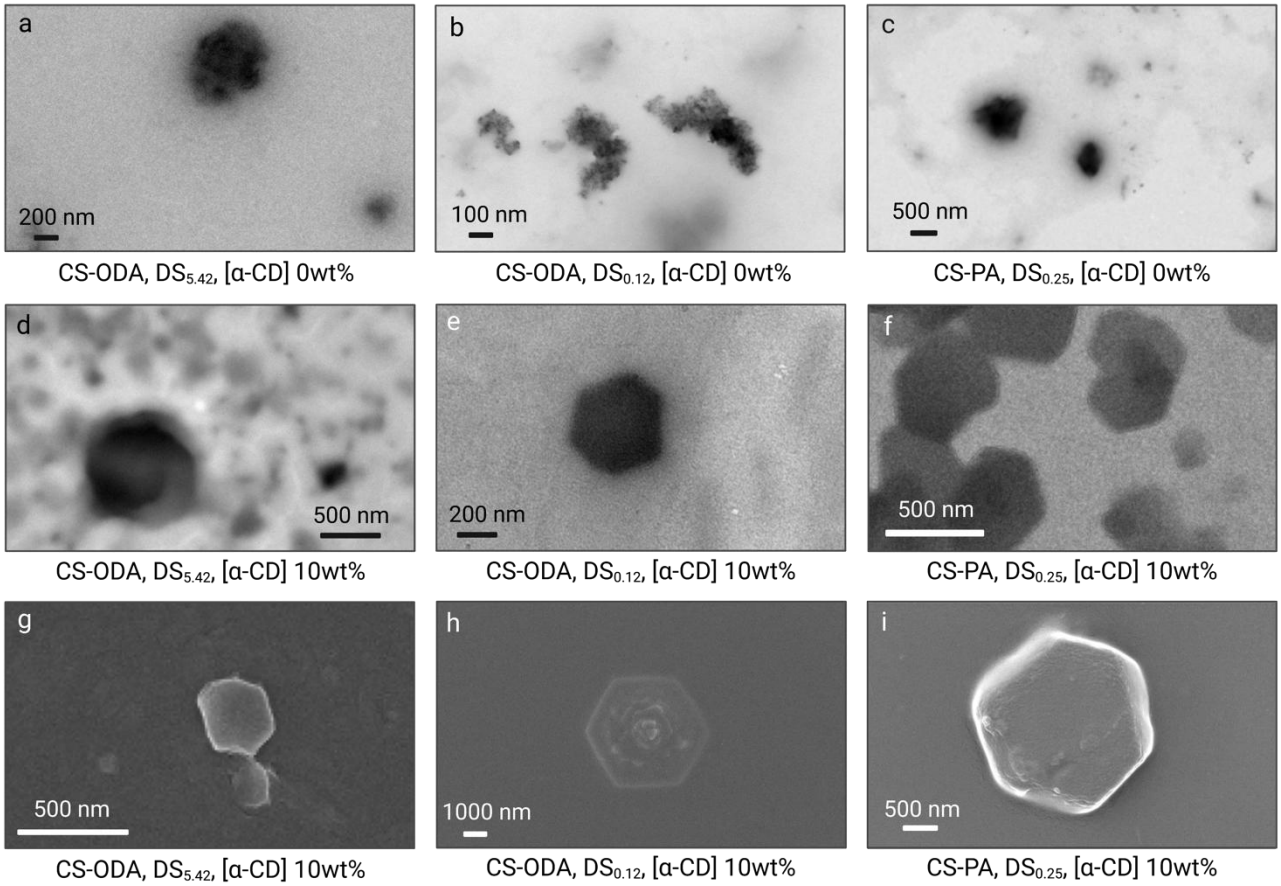

Figure 1. TEM and SEM pictures of particle suspensions obtained with CS-ODA and CS-PA. Hydrophobically modified CS were used at a concentration of (1 wt%) without α-CD or in the presence of α-CD at a concentration of 10 wt% in water. The suspensions were diluted in water (1/33) before observation.

Table 2. a) Zeta potentials (ζ) of hydrophobically modified polysaccharide suspensions and NP. Results are expressed as the mean ± SD (nm). Three measurements were performed for each formulation. b) IC_{30}, and c) IC_{50} values (μg mL^{-1}) at 24 h for GAG preparations after fitting to a dose-response curve in two different cell lines. All experiments were repeated three times. The IC_{50} and IC_{30} were obtained from Figures 3, 4, and S7 in the Supporting Information.

GAG preparation	DS_{NMR} (%)	α-CD wt%		a	b		c	
				ζ (mV) ± SD	IC_{30} (μg mL^{-1})		IC_{50} (μg mL^{-1})	
					J774A.1	HUCs	J774A.1	HUCs
CS	-	-	Solution	-	36	> 500	> 500	> 500
CS-ODA	5.42	0	Suspension	-37.0 ± 2.0	0.4	18	3.2	68
		10	NP	-44.3 ± 0.7	0.38	11	8.7	19
	0.12	0	Suspension	-31.4 ± 4.6	5	183	34.4	337.5
		10	NP	-40.2 ± 1.8	3.7	100	36.1	> 500
CS-PA	0.25	0	Suspension	-31.1 ± 5.8	39	>500	> 500	> 500
		10	NP	-47.1 ± 2.0	8.5	35	220.6	> 500
HEP	-	-	Solution	-	> 500	> 500	> 500	> 500
HEP-ODA	3.25	0	Suspension	-46.8 ± 1.6	0.6	24	1.9	38.7
		10	NP	-48.9 ± 0.2	0.4	3.6	1.4	7.13
	0.28	0	Suspension	-50.3 ± 3.0	2.1	78	56.3	> 500
		10	NP	-51.6 ± 1.5	1.4	27	36.1	191.3
HEP-PA	0.15	0	Suspension	-43.3 ± 1.1	94	> 500	202.5	> 500
		10	NP	-46.7 ± 3.3	16	115	50.5	> 500
HA	-	-	Solution	-	> 500	> 500	> 500	> 500
HA-PA	0.12	0	Suspension	-32.8 ± 2.6	27	333	459	> 500
		10	NP	-37.3 ± 1.9	21	70	245	447

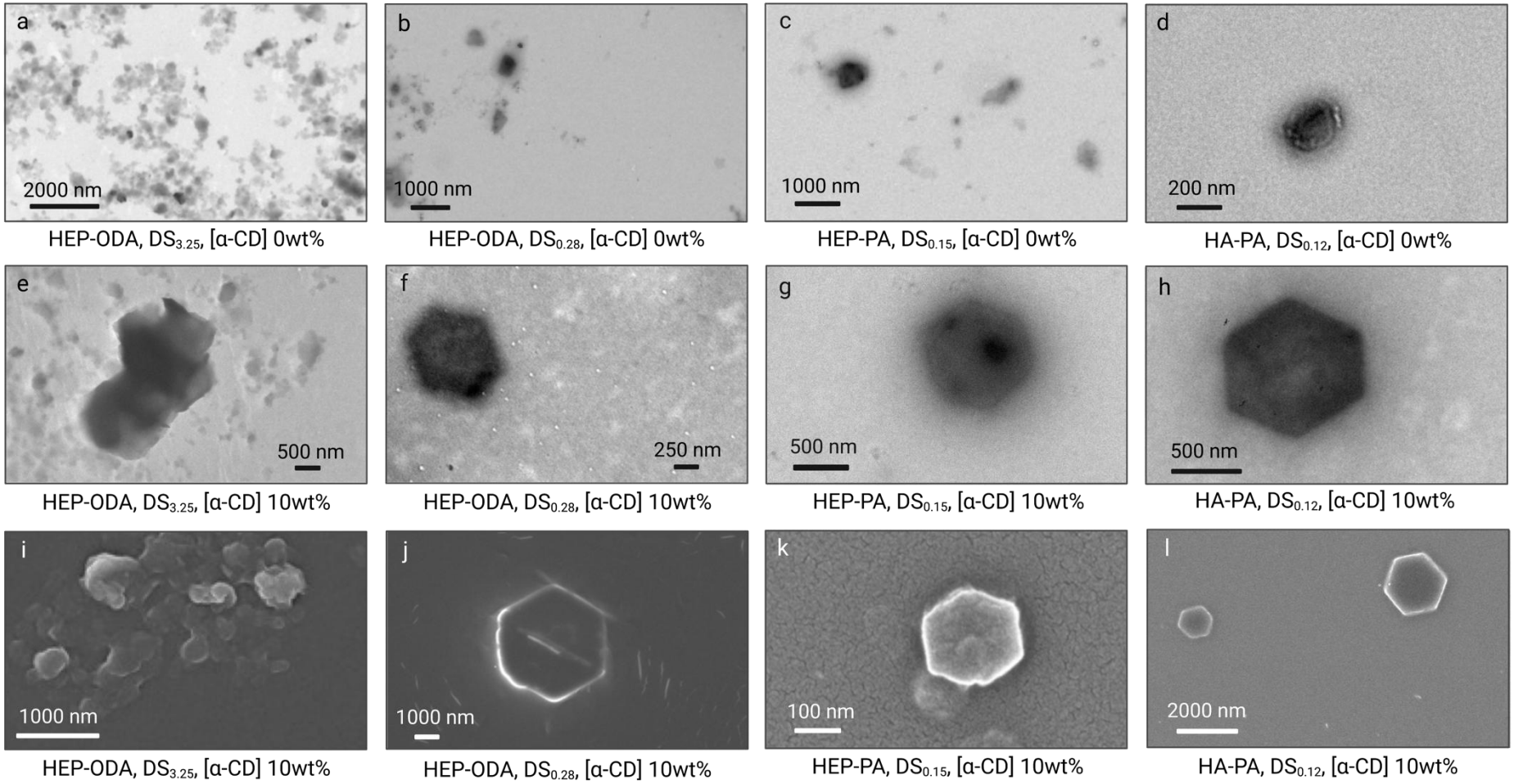

Figure 2. TEM and SEM pictures of particle suspensions obtained with HEP-ODA and HEP-PA. Hydrophobically modified HEP or HA were used at a concentration of (1 wt%) without α-CD or in the presence of α-CD at a concentration of 10 wt% in water. The suspensions were diluted in water (1/33) before observation.

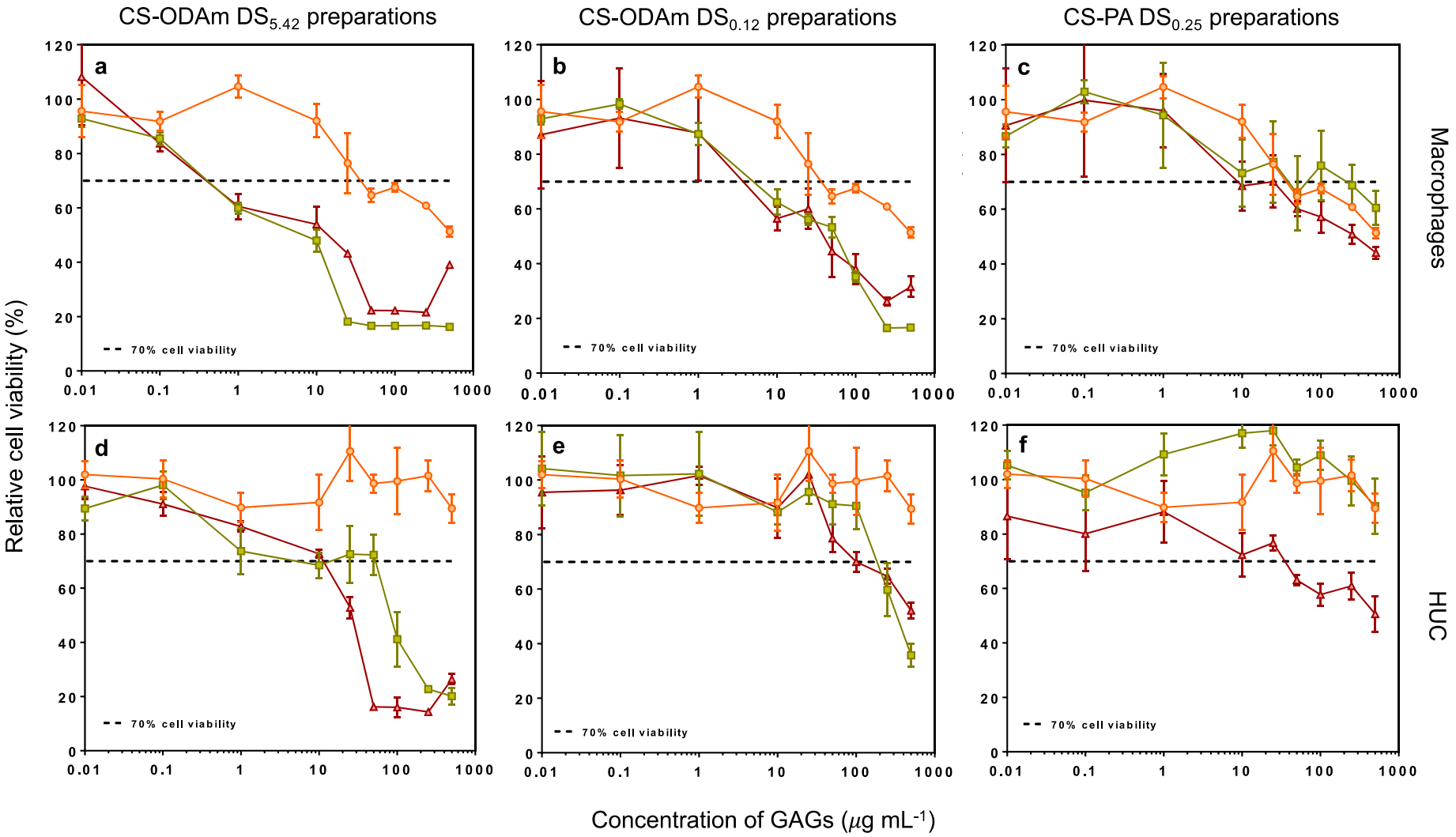

Figure 3. Cell viability testing of solutions of CS (circle, orange), hydrophobically modified CS suspensions (square, green), and CS NP (triangle, red). Dose-response data show the cytotoxicity to macrophages (a,b,c), and HUC (d,e,f). The two cell lines were exposed to different concentrations (0.01, 0.1, 1, 10, 25, 50, 100, 250, and 500 μg mL^{-1} of GAG. (a,d) CS-ODA $DS_{5.42}$, (b,e) CS-ODA $DS_{0.12}$, (c,f) CS-PA $DS_{0.25}$. The dotted lines show 70% of cell viability. Data are presented as the mean ± s.d. ($n = 6$ independent experiments).

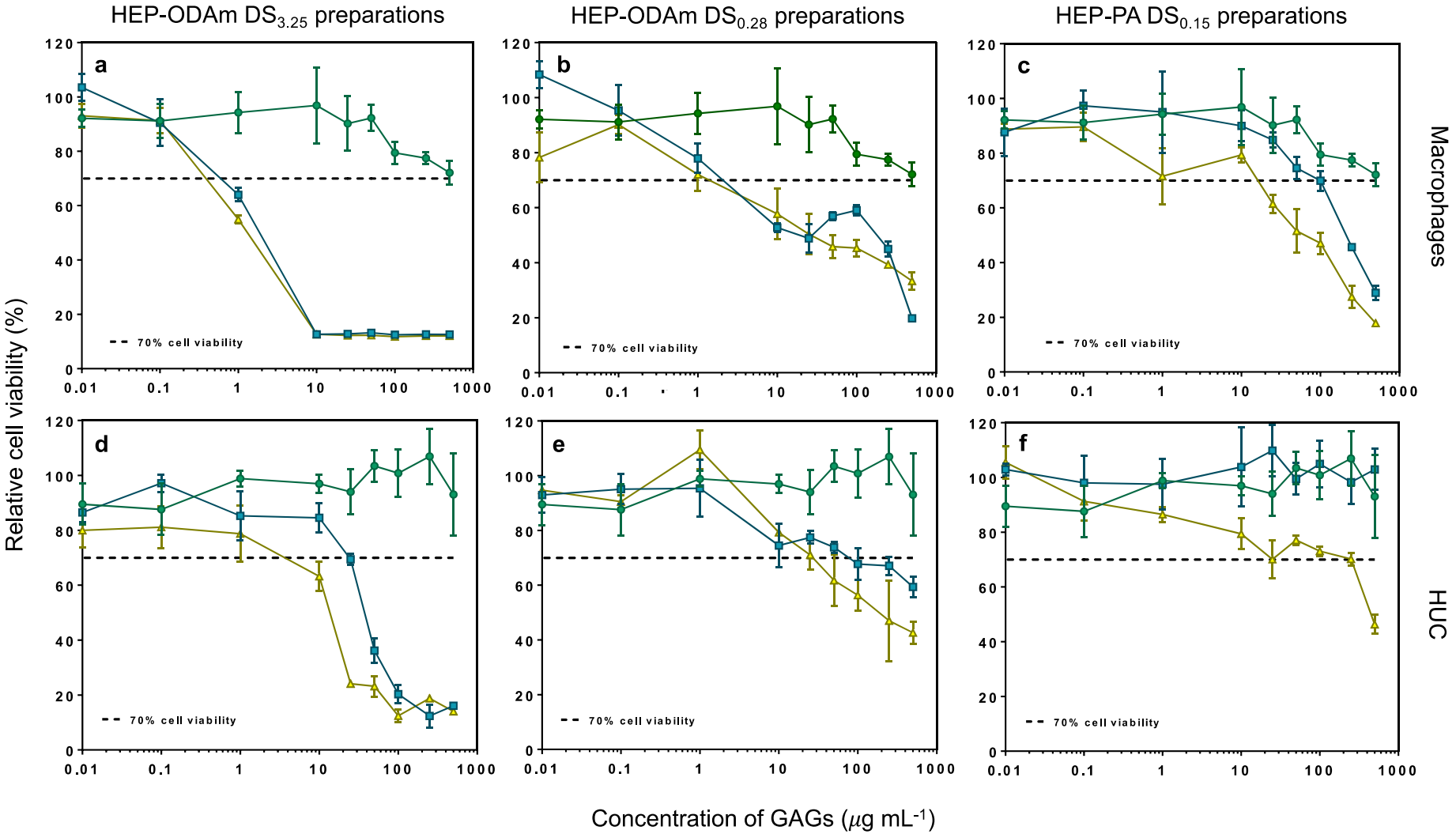

Figure 4. Cell viability testing of solutions of HEP (circle, dark green), hydrophobically modified HEP suspensions (square, dark turquoise blue), and HEP NP (triangle, light green). Dose-response data show the cytotoxicity to macrophages (a,b,c), and HUC (d,e,f). The two cell lines were exposed to different concentrations (0.01, 0.1, 1, 10, 25, 50, 100, 250, and 500 µg mL^{-1} of GAG. (a,d) HEP-ODA $DS_{3.25}$, (b,e) HEP-ODA $DS_{0.28}$, (c,f) HEP-PA $DS_{0.15}$. The dotted lines show 70% of cell viability. Data are presented as the mean ± s.d. ($n = 6$ independent experiments).

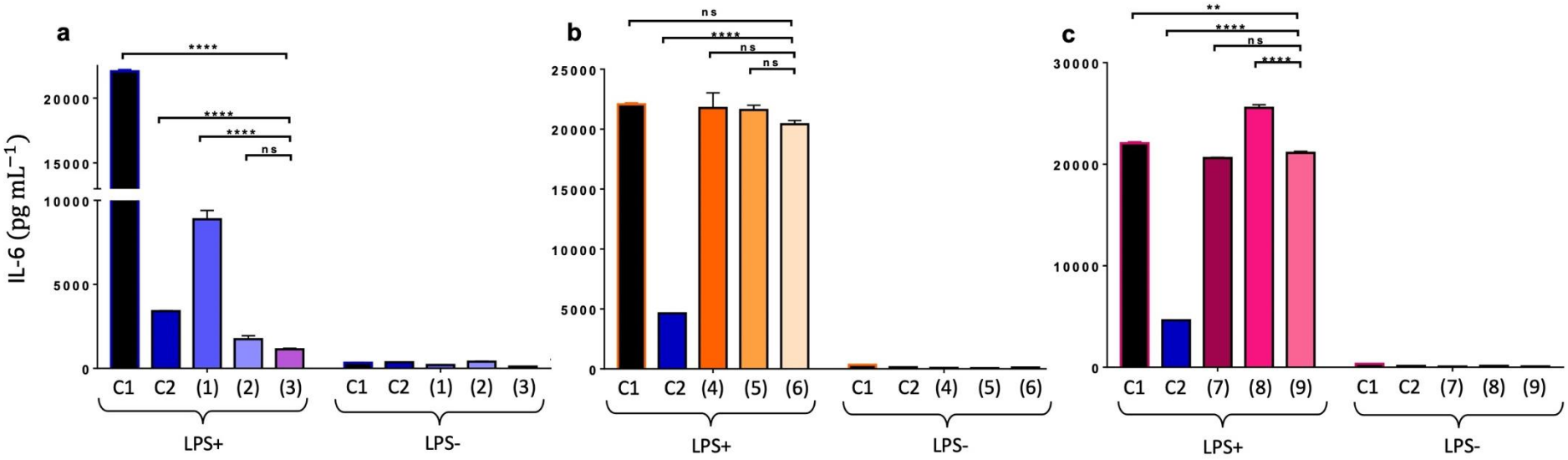

Figure 5. Concentration of IL-6 cytokine produced by macrophages with LPS induction (LPS+) or without LPS induction (LPS-) after treatment with preparations composed of HA (a), CS (b), and HEP (c). GAG were used at a concentration of 25 μg mL^{-1}. Samples treated with PBS were the positive controls of inflammation (C1). Dexamethasone was used as a reference anti-inflammatory drug (C2). GAG preparations were HA solution (1), HA-PA suspension (2), HA NP (3), CS solution (4), CS-PA suspension (5), CS NP (6), HEP solution (7), HEP-PA suspension (8) or HEP NP (9). One, two, three, and four asterisks denote *p*-values < 0.05; < 0.01; < 0.001 and < 0.0001 respectively, after one-way ANOVA followed by Tukey's multiple comparison post-test comparing the mean between different groups. No statistical significance was denoted by ns. Results are presented as mean ± SEM ($n = 3$ independent experiments).

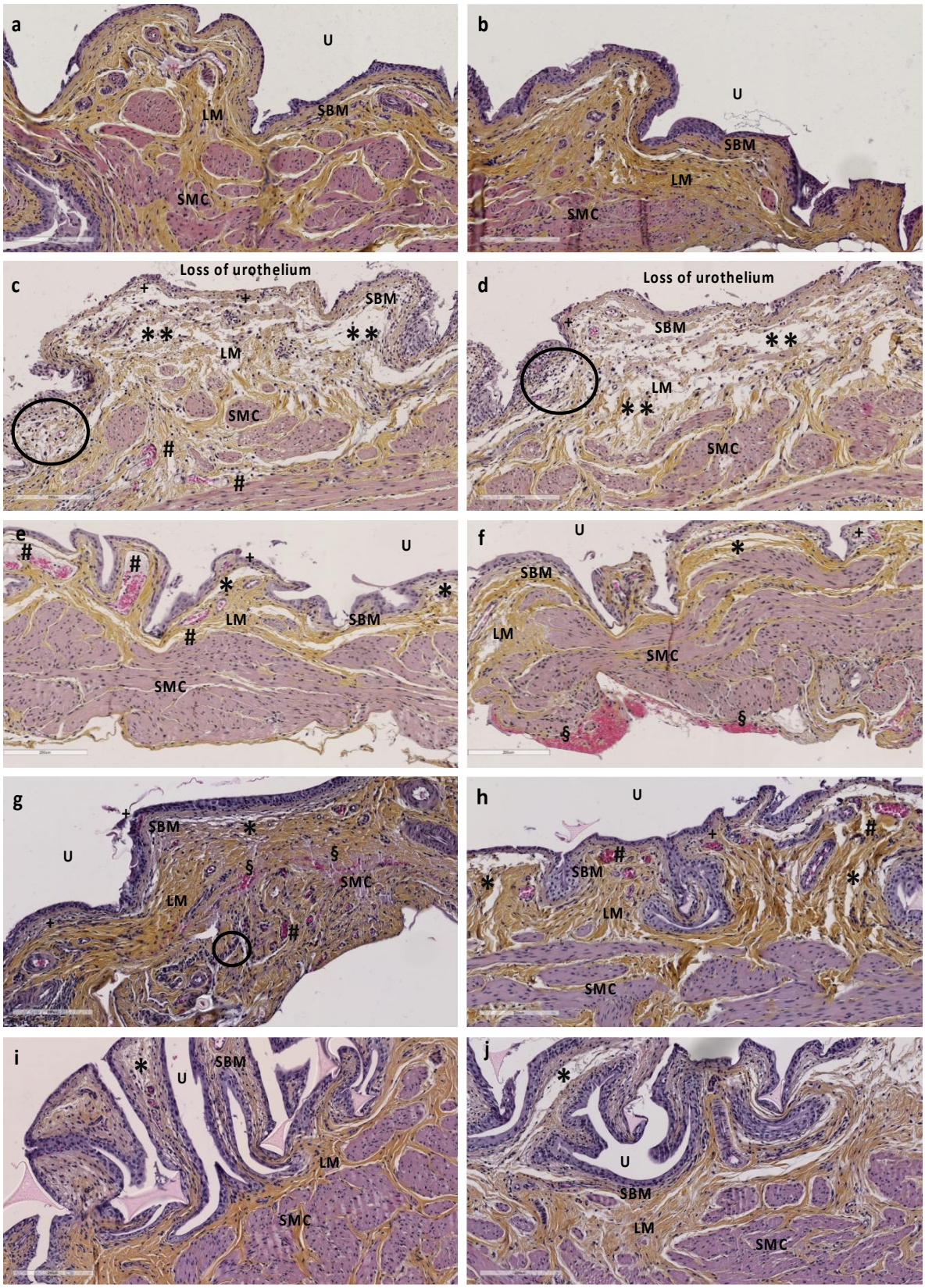

Figure 6. HES-stained high-resolution scans of bladders collected from healthy rats (a,b) or from rats after intravesical instillation of LPS/PS (c,d). HA preparations were administered as HA solution (e,f), HA-PA suspension (g,h), or HA NP (i,j) at a concentration of 10 mg mL^{-1} in HA. # veinous congestion. *Circles*, leucocytes infiltration. §, hemorrhage. +, urothelial thinning or ulceration. *, mild edema. **, moderate edema. *U*, urothelium. *SBM*, submucosa. *LM*, lamina propria. *SMC*, smooth muscle cell layer. Scale bar represents 200 µm

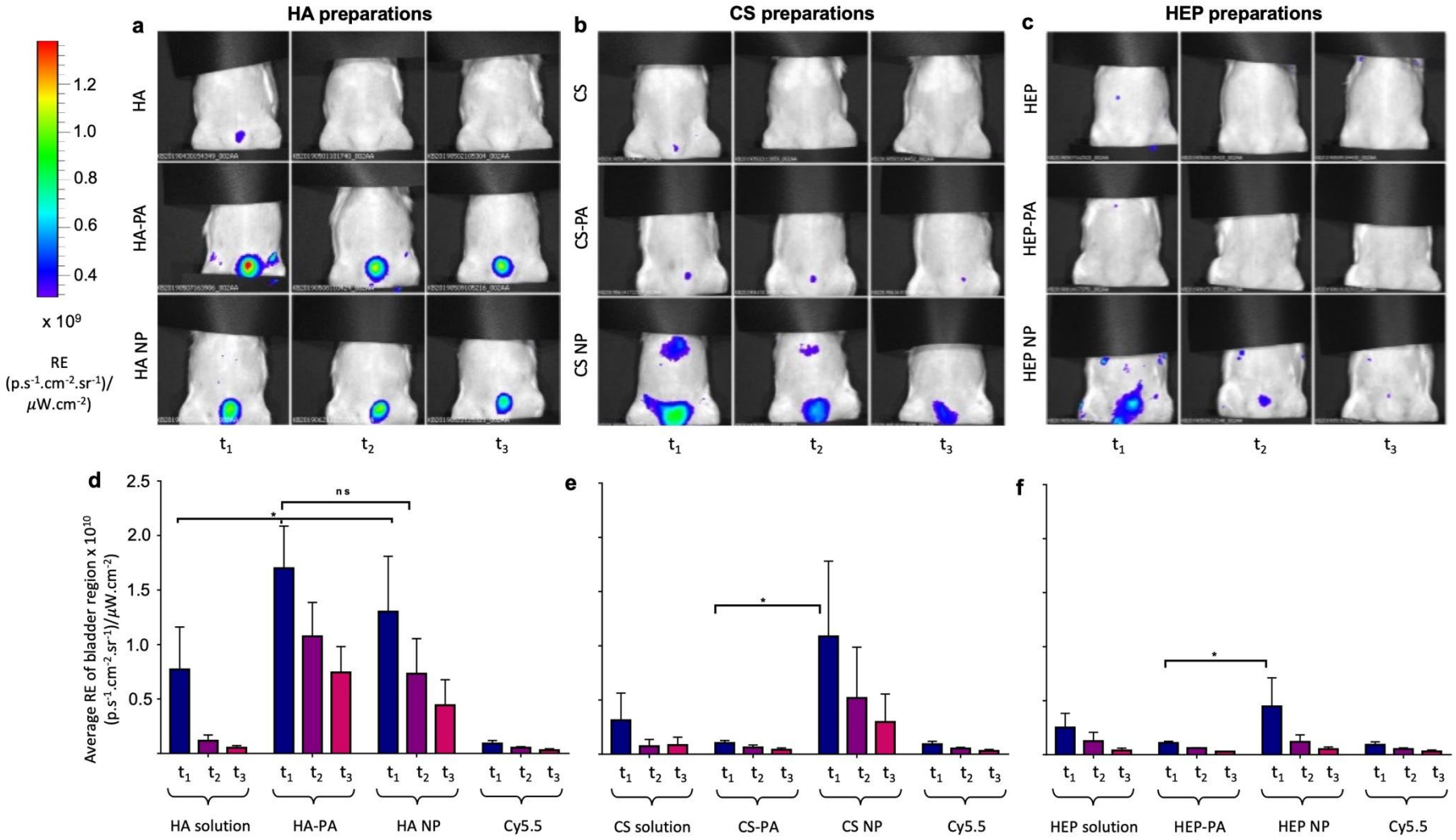

Figure 7. (a,b,c) IVIS Lumina scans and (d,e,f) average radiant efficiency (RE) of rat abdomens after 24 h (t_1), 48 h (t_2), and 72 h (t_3) postadministration of preparations composed of HA (a,d), CS (b,e) and HEP (c,f). GAG preparations were HA solution (1), HA-PA suspension (2), HA NP (3), CS solution (4), CS-PA suspension (5), CS NP (6), HEP solution (7), HEP-PA suspension (8) or HEP NP (9). GAG were used at a concentration of 10 mg mL^{-1}. Rats treated with a solution of Cy5.5, are used as a control (C). One asterisk denoted p-value < 0.05 after two-way Kruskal-Wallis test followed by a Tukey's multiple comparison post-test. $n = 3$ rats for each group.

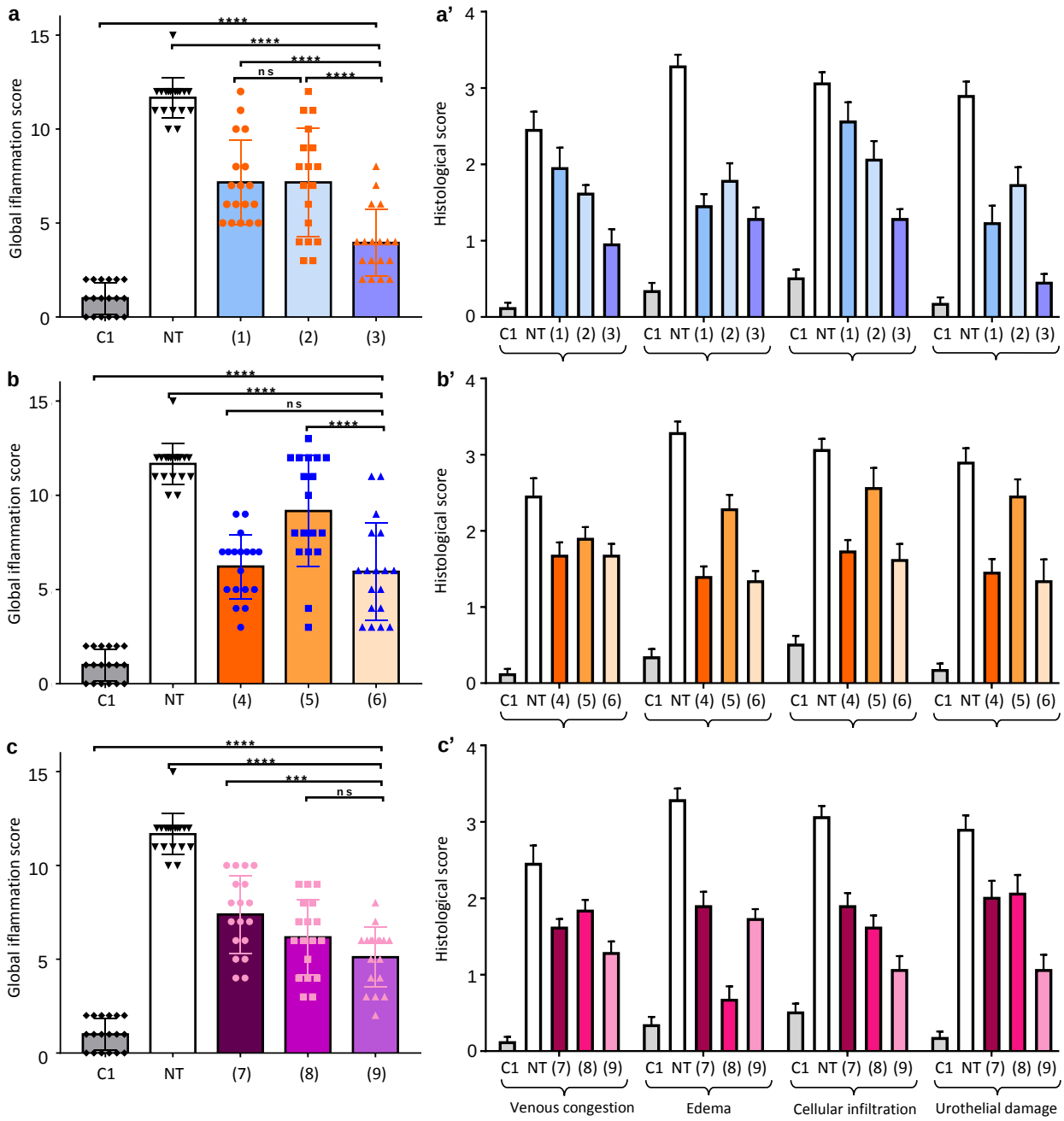

Figure 8. (a,b,c) Global inflammation scores obtained from the analysis of high-resolution scan images of the bladder inflammation 72 h postadministration of preparations composed of HA (a), CS (b), or HEP (c). GAG preparations were HA solution (1), HA-PA suspension (2), HA NP (3), CS solution (4), CS-PA suspension (5), CS NP (6), HEP solution (7), HEP-PA suspension (8) or HEP NP (9). C1 represents the healthy rat group, and NT represents the non-treated rat group in which the inflammation was induced. Tissues were scored from 0 to 4 for venous congestion, edema, cellular infiltration, and urothelial damage (a',b',c'), giving a maximal histological score of 16 per slide. Statistical analysis was performed with two-way ANOVA followed by Tukey's post-test. One, two, three, and four asterisks denoted *p*-value < 0.05, < 0.01, < 0.001, and < 0.0001, respectively. No significant differences were denoted by ns. $n = 3$ rats for each group, and 6 images for each group were analyzed.